Design and Experimental Characteristics of an Erbium Doped GaN Waveguide

By

Qian Wang

Submitted to the graduate degree program in the Department of Electrical Engineering and Computer Science and the Graduate Faculty of the University of Kansas in partial fulfillment of the requirements for the degree of Master of Science.

_____

Chairperson Professor Rongqing Hui

_____

Professor Kenneth R. Demarest

_____

Professor Christopher Allen

Date Defended: April 17th 2012

The Thesis Committee for Qian Wang

certifies that this is the approved version of the following thesis:

Design and Experimental Characteristics of an Erbium Doped GaN Waveguide

_____

Advisor/Chairperson: Rongqing Hui

Date approved:

ABSTRACT

The goal of this research was to develop an optical amplifier based on Erbium doped GaN waveguides, which can be used in the next-generation of planar integrated optic circuits. This thesis started from the basic concepts of fiber optic communication systems, attenuation of optical signals, principles of optical amplifiers and planar optical waveguides. We focused on the principles and applications of Erbium doped fiber amplifiers (EDFA) and the physical properties of Er: GaN waveguides.

This thesis reports the characteristics of an erbium-doped GaN semiconductor waveguide amplifier grown by metal-organic chemical vapor deposition (MOCVD). We demonstrated that both 980 and 1480 nm optical pumping were efficient to create population inversion between the $^4I_{13/2}$ and $^4I_{15/2}$ energy levels. The carrier lifetime in the $^4I_{13/2}$ energy band was measured to be approximately 1.5 ms in room temperature, which is slightly shorter than that in erbium-doped silica due to the interaction between the erbium ions and the semiconductor lattice structure. But it is significantly longer than the carrier lifetime in a typical semiconductor optical amplifier which is in the nanosecond regime. The emission cross section was obtained with the Füchtbauer–Ladenburg (FL) equation based on the measured spontaneous emission and the radiative carrier lifetime. The absorption cross section was derived from the emission cross section through their relation provided from the McCumber's theory. The conversion efficiency from a 1480nm pump to 1537nm emission was measured, which reasonably agreed with the calculation based on the emission and absorption cross section.

ACKNOWLEDGEMENTS

I would like to express my gratitude to Dr. Rongqing Hui, my committee chair, for his guidance throughout this research work and for his precious advice and support during my graduate studies here at the University of Kansas. I also thank him for providing me with the necessary motivation and interest all throughout the course of the project. This thesis would have been incomplete without his invaluable input and timely reviews.

I would also like to express appreciation to the other members of my committee, Dr. Christopher Allen and Dr. Kenneth Demarest, for serving on my thesis committee and giving me invaluable suggestions. Also, I would like to thank Dr. Hongxin Jiang from Texas Tech University and Dr. Judy Wu from the Department of Physics (KU) for their help throughout my research work. I would like to express my thanks to the National Science Foundation for providing the financial support for my research work.

Finally, I would like to thank my family and friends for their patience and encouragement throughout the work of my dissertation. The support from them makes this work successful.

Contents

LIST OF FIGURES

INTRODUCTION

Optical fiber is an ideal medium which can be used to carry optical signals over long distances. After being first developed in the 1970s, fiber-optic communication systems have played a major role in the advent of the Information Age [1]. Due to its advantages over electrical transmission, optical fiber has largely replaced copper wires in core communications networks nowadays [2].

In current lightwave systems, the repeater spacing is increased by the use of optical amplification, and the use of wavelength-division multiplexing (WDM) enabled the full use of the optical fiber bandwidth. In fact, after 1992 the advent of the WDM technique resulted in a revolution of the system capacity and led to lightwave systems operating at a bit rate of 10 Tb/s by 2011 [3].

It is well known that attenuation is one of the most important parameters of an optical fiber, which determines how far an optical signal can be delivered while still maintains a detectable power level at the receiver. Several factors contribute to fiber attenuation, such as absorption, scattering and radiation. Material absorption results from photon-induced molecular vibration, which absorbs signal optical power and turns it into heat. Although pure silica molecules have very low absorption in the wavelength band from ultraviolet (UV) to near infrared (NIR), impurities inside silica material such as OH^- ions may be introduced in the fiber fabrication process, which create wavelength-dependent absorption in the fiber. There exist high absorptions around 700nm, 900nm and 1400nm for OH^- ions, which are commonly referred to as water absorption peaks.

Scattering loss arises from silica molecules, fiber structural in-homogeneities and microscopic defects. In general, the optical characteristics of scattering depend on the size of the scatter in comparison to the signal wavelength. For the molecular scattering, since the scatters are much smaller than the signal wavelength, it is usually characterized as Rayleigh scattering, which contributes to an intrinsic attenuation in the fiber. A very important spectral property of Rayleigh scattering is that the scattering loss is inversely proportional to the fourth power of the wavelength. Therefore, Rayleigh scattering loss is high in short wavelength region. The following figure shows the contribution of the above factors to the total fiber loss.

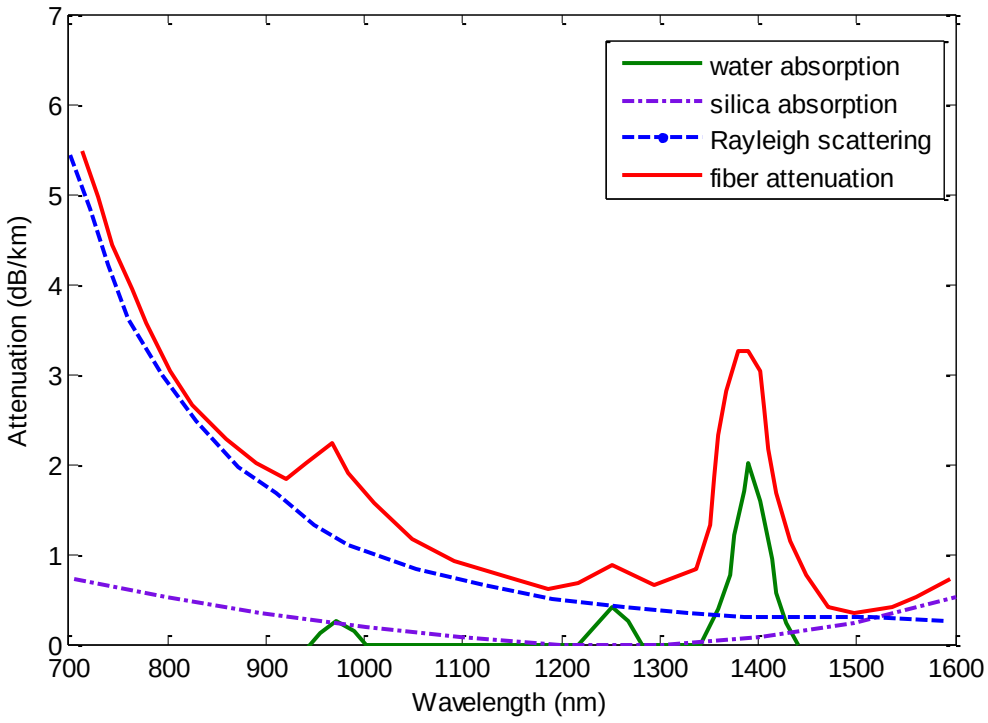

Figure 1-1 typical absorption spectra of silica fiber (including water absorption, silica absorption and Rayleigh scattering). There is a local minima of attenuation at 1500nm wavelength window.

In this spectrum, there are three local minima in 850nm, 1310nm and 1550nm, which have been used as the main wavelength windows for optical communications. I will focus on the 1550nm wavelength window in this thesis because of its lowest attenuation.

Optical amplifier is important in optical communication and laser physics, which is a device that can amplify an optical signal directly, without the need to first convert it to an electrical signal. Several different physical mechanisms are used to amplify a light signal. In optical amplifiers and lasers, stimulated emission is the basic mechanism which introduces amplification of incoming signal photons in the gain medium [5]. Semiconductor optical amplifiers (SOAs) are essentially laser diodes without end mirrors, which are electrically pumped to create carrier population inversion. We can think of a SOA as a laser without an optical cavity or one in which feedback from the cavity is suppressed. Erbium doped fiber amplifiers (EDFAs) utilize Erbium doped fibers as gain medium and the carrier population inversion is achieved by optical pumping. However, Raman optical amplifiers are based on stimulated Raman scattering (SRS) to create optical gain, which is a different phyical principle than EDFA or conventional lasers. I will talk about semiconductor optical amplifiers (SOAs) and Er doped optical amplifiers in this thesis, and focus on the Er doped GaN amplifiers [6-9].

InGaAsP-based traveling wave semiconductor optical amplifier (SOA) is electrically pumped and monolithically integratable with other components such as laser sources. However, due to the short carrier lifetime of a SOA, cross-saturation may cause significant inter-channel crosstalk between different wavelength channels, which is a major problem preventing its practical applications in WDM systems. In fact, short

lifetime is intrinsic to free carriers involved in the interband recombination in most semiconductors.

Erbium (Er)–doped materials have attracted much attention for their application in photonics, especially in the area of optical communications. Doped in a solid host, Er^{3+} ion has allowable intra-4f shell transition from its first excited state ($^4I_{13/2}$) to the ground state ($^4I_{15/2}$) and the transition corresponds to a wavelength of minimum optical loss in silica based optical fibers (1.55um). Thus, Er-doped materials are ideal candidates to make amplifiers for optical communications. Today, Er-doped fiber amplifiers (EDFAs) are widely used in long-haul fiber-optic communications for compensating the loss of long fiber spans.

III-nitride semiconductors are excellent host materials for Er-ions due to their structural and thermal stabilities. III-nitride wide bandgap semiconductors have recently attracted much attention because of their applications in blue/UV optoelectronic devices as well as high power, high temperature electronic devices. Optical emission in 1.55 um wavelength window in Er-doped GaN films has been observed. In particular, GaN and AlGaN epilayers doped with Er-ions have demonstrated a highly reduced thermal quenching of the Er luminescence intensity from cryogenic to elevated temperatures as compared to other semiconductor host materials such as Si and GaAs. 1540nm optical emission in Er-doped waveguide has also been demonstrated using a 365nm light emitting diode as the optical pumping source. UV pumping above the GaN bandgap excited free electrons and holes, and subsequently the electronics and holes transfer their energy to the doped erbium ions and produce sufficient carrier population on the $^4I_{13/2}$

band which is responsible for emission in the 1550nm wavelength window. This above bandgap excitation was demonstrated to be more efficient than below bandgap excitation. In this thesis, both the dynamic excitation mechanism in Er doped GaN materials and the design of GaN waveguides are discussed. [10, 11]

Although both 980nm and 1480nm optical pumping can be used in EDFAs in fiber-optic systems, investigations in Er-doped GaN so far were limited to the use of either green pump source in 530nm wavelength window or UV pumping at 350nm. In fact, pumping at near infrared wavelengths to populate carriers in $^4I_{13/2}$ energy band would have an advantage of providing higher photon conversion efficiency than using higher energy photons such as in UV and green wavelengths, which also avoided transitions through intermediate energy levels and the associated energy loss during these transitions [13-16].

It is obvious that the understanding of stimulated emission in Er-doped GaN can be further improved by modeling key parameters such as carrier lifetime, absorption and emission cross-sections (CSs). Carrier lifetime is defined as the average time it takes for a minority carrier to recombine. Although the carrier lifetime of Er in Silica fibers has been measured to be around 10ms, the carrier lifetime of Er doped in GaN has never been measured, which is an important question this research is trying to address.

Transition cross sections are used to quantify the likelihood of optically induced transition events. In order to guarantee a stimulated emission from an optically pumped amplifier, the material needs to have maximum absorption CS at the pump wavelength and a high emission CS at the signal wavelength.

There are many ways for determining the CSs of rare earth ions in semiconductor hosts. But in general, since it was difficult to directly measure both the absorption cross section σ_a and the emission cross section σ_e, the typical procedure was to measure σ_a first and then calculate σ_e based on the measured results of σ_a using the Einstein A and B coefficients for a two level system. In such an approach, the transition strength is sensitive to the Stark levels involved according to low temperature absorption and emission measurements. Therefore the above condition is not satisfied for Er:GaN at room temperature due to different populations on the sub-levels of each state, which made us approach the problem of calculating CSs in a different way [12].

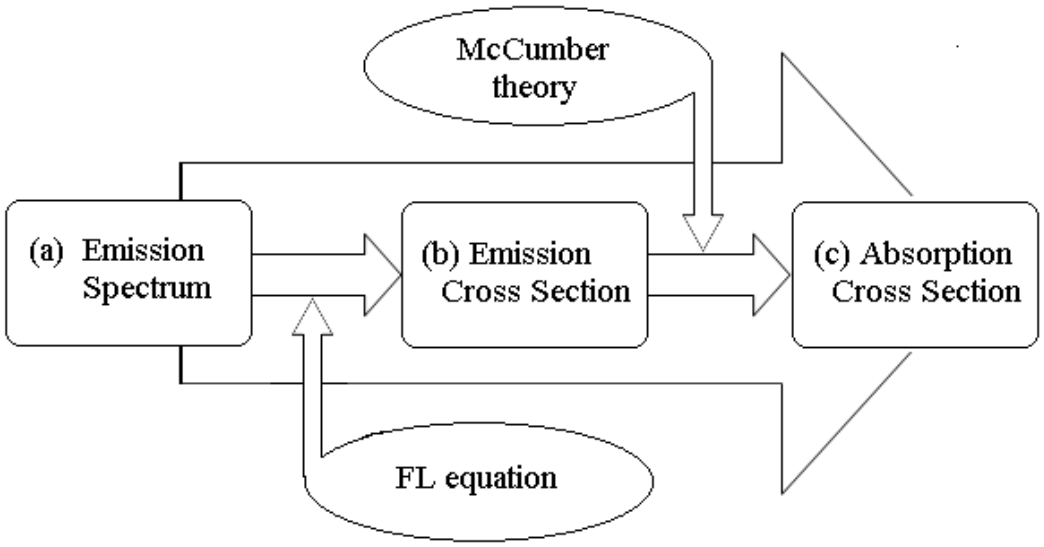

Figure 1-2 Flowchart showing the calculation procedure of absorption cross-section from emission spectrum. Starting from the measurement of spontaneous emission spectrum, we used FL equation and McCumber's theory to determine the emission cross section and absorption cross section.

The only requirement for the theory of McCumber is that the time necessary to establish a thermal distribution with each manifold should be short compared with the lifetime of that manifold [7]. In our approach, we first measure the spontaneous emission spectrum and the spontaneous emission carrier lifetime from the Er-doped waveguide. The emission cross section can be obtained with the Füchtbauer–Ladenburg Equation based on the measured spontaneous emission spectrum and the carrier lifetime. Then, the absorption cross section can be derived from the emission cross section through their relation provided from the McCumber's theory. Figure.1.2 shows the flowchart of the calculation procedure of absorption cross-section from the spontaneous emission spectrum.

In the following sections, I will provide mode detailed information about the theoretical and experimental approaches we used, the problems we faced, the data we collected, theoretical analysis we performed and our proposed improvements for each technique in the future.

THEORETICAL BACKGROUND

2.1 The principle of EDFA

An optical amplifier is a device that directly amplifies the optical signal, without the need to convert it to electrical signal. Optical amplifiers have found widespread use not only in long-distance point-to-point optical fiber links, but also in multi-access optical networks to compensate for signal splitting losses.

There are two main types of optical amplifiers, which are semiconductor optical amplifiers (SOAs) and Erbium doped fiber amplifiers (EDFAs). Like in a laser, the most important component of an optical amplifier is the gain medium, but optical feedback is not required in an optical amplifier and the optical signal passes through the gain medium only once. Optical amplifiers amply the optical signal through the stimulated emission process in the gain medium where carrier density is inverted. At the same time, there is also spontaneous emission in the gain medium, which creates optical noise in addition to the amplified signal.

SOA is electrically pumped and the gain is usually achieved by electronical current injection. Electrons are injected from an external current source into the active region of the gain medium. These energized electrons occupy energy states in the conduction band (CB), leaving holes in the valence band (VB). If a photon of suitable energy goes into the active region, it can cause stimulated recombination of a CB electron and a VB hole, generating a new stimulated photon with identical phase and frequency with the incident photon. At the same time, electrons from the excited state can also

recombine with the valance band holes spontaneously generating spontaneous photons. These spontaneously generated photons have random phase and with a wide range of frequency. In fact this spontaneous emission is essentially a noise process which also reduces the optical gain by reducing the excited state carrier population. The carrier lifetime of an SOA is really short because it mainly depends on the band-edge recombination in the semiconductor. Due to its short carrier lifetime, optical gain in an SOA is able to change very quickly, so that fast gain dynamics is one of the unique properties of semiconductor optical amplifiers in comparison with fiber amplifiers which will be discussed later. SOA is often used to accomplish all-optical switch in optical networks due to its high-speed cross gain saturation mechanism. At the same time it may introduce crosstalk between different wavelength channels through the same mechanism, which limits its practical applications in WDM systems. Erbium doped fiber amplifier (EDFA) is one of the most popular optical devices in modern optical communication systems as well as in fiber-optic instrumentation. EDFAs provide many advantages compared to SOAs in terms of high gain, high optical power, low crosstalk between wavelength channels and easy optical coupling from and to optical fibers. In contrast to SOA, an EDFA is optically pumped and therefore it requires a pump source which is usually a high power semiconductor laser. The basic structure of an EDFA is shown in Fig.2.1, which is composed of an erbium doped fiber, a pump laser, an optical isolator and a wavelength-division multiplexer. The wavelength division multiplexer (WDM) is used to combine the short wavelength pump with the longer wavelength signal. Since an EDFA may provide significant amount of optical

reflection may be able to cause oscillation and therefore degrade EDFA performance, so an optical isolator is usually used to minimize the impact of reflections.

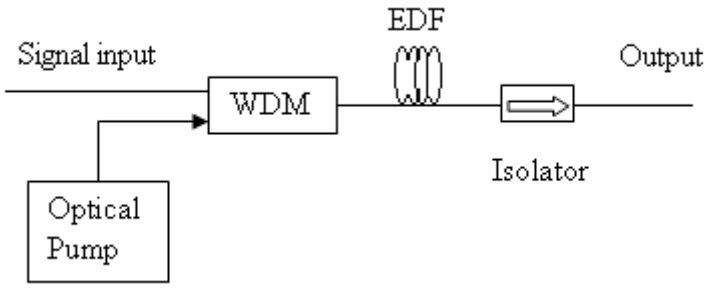

Figure 2-1 Setup of Erbium Doped Fiber Amplifier, which utilizes an Er doped fiber as the gain medium

The general energy band structure of the rare-earth element Erbium and its inner shell transitions are shown in Figure 2.2.

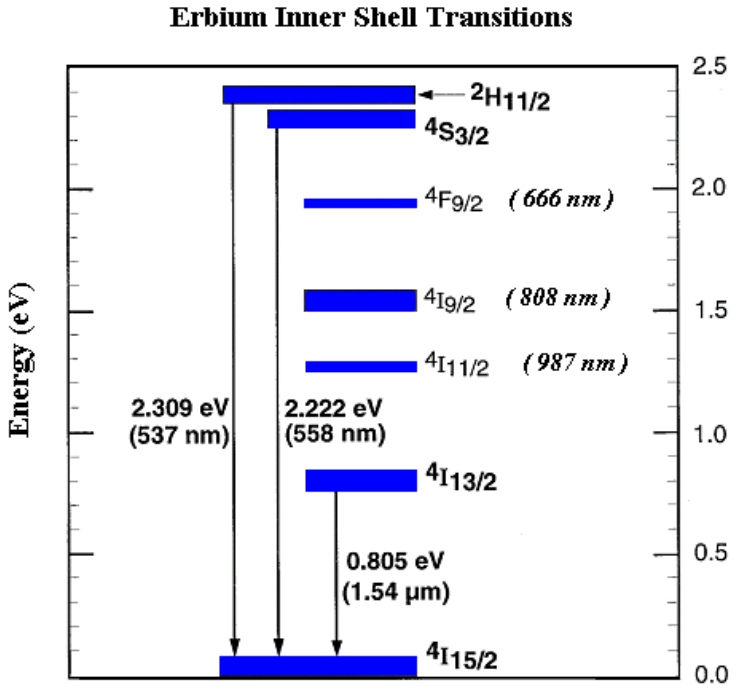

Figure 2-2 General band structure of Erbium and its inner shell transitions

Optical pumping process in an erbium doped fiber is usually described by a simplified three level energy system as illustrated in Fig.2.3 (a).

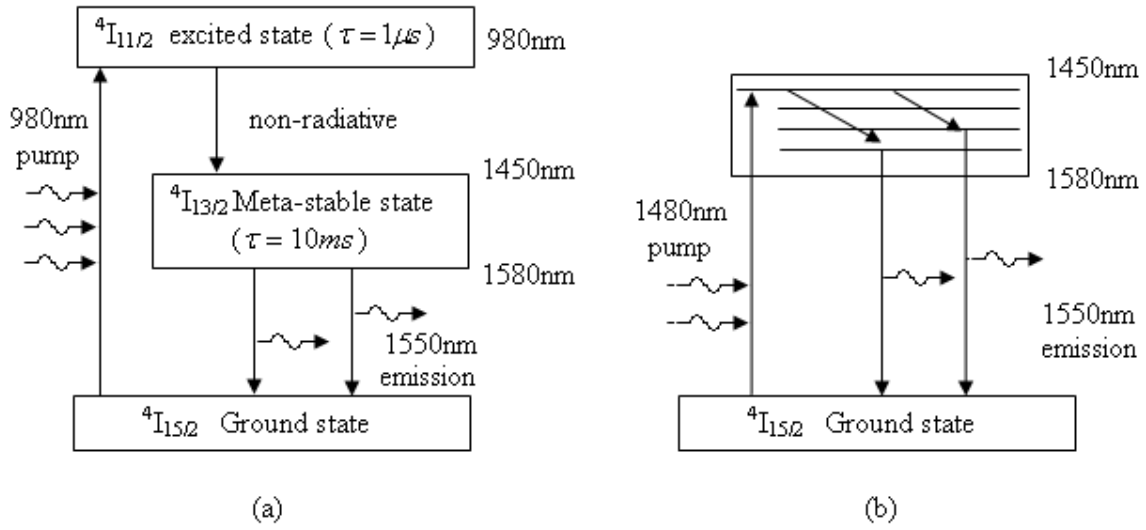

Figure 2-3 Simplified energy band diagrams of Erbium ions in silica. Fig (a) shows the 3-level energy band structure including 1st excited state. Fig (b) shows the 2-level energy band structure of metastable state and ground state.

The bandgap between the ground state and the excited state is approximately 1.268eV, therefore pump photons at 980nm wavelength are able to excite ground state carriers to the excited state and create population inversion. The carriers stay in the excited state for only about 1us, and after that they decay into a metastable state through a non-radiative transition. In this process, the energy loss is turned into mechanical vibrations in the fiber. The energy band of the metastable state extends roughly from 0.8eV to 0.84eV, which corresponds to a wavelength band from 1480nm to1550nm. Finally, radiative recombination happens when carriers step down from the metastable state to the ground state and emit photons in the 1550nm wavelength region. The carrier

lifetime in the metastable state is in the order of 10ms for typical silica fibers, which is 4 orders of magnitude longer than the carrier lifetime in the excited state. Therefore, with constant optical pumping at 980nm, almost all the carriers will be accumulated in the metastable state, and the three-level system can be simplified into two levels for most of the practical applications, as shown in Fig.2.3 (b).

An erbium doped fiber can also be pumped at 1480nm wavelength, which corresponds to the bandgap between the top of metastable state and the ground state. In this case, 1480nm pump photons excite carriers from ground state to the top of metastable state directly. Then these carriers relax down to the bottom part of the metastable band. Typically, 1480nm pumping is more efficient than 980nm pumping because it does not involve the non-radiative transition from 980nm to 1480nm band. Therefore, 1480nm pumping is often used for high power optical amplifiers. However, amplifiers with 1480nm pump usually have higher noise figure than 980nm pump.

2.2 Evaluation of EDFA

Absorption and emission cross-sections are two very important properties of erbium-doped fibers. The name "cross-section" has nothing to do with the geometric cross-section of the fiber. The physical meanings of absorption and emission cross-sections in an EDFA are absorption and emission efficiencies as the function of wavelength. Let's start with the pump absorption efficiency W_p, which is defined as the probability of each ground state carrier that is pumped to the metastable state within each second. If the pump optical power is P_p, within each second the number of incoming pump photons is P_p/hf_p, where f_p is the optical frequency of the pump. Then, pump absorption efficiency is $W_p = \frac{\sigma_a P_p}{hf_p A}$, where A is the effective fiber core cross section area and σ_a is the absorption cross section. In another word, the absorption cross-section is defined as the ratio of pump absorption efficiency and the density of pump photon flow rate: $\sigma_a = \frac{W_p}{(P_p / hf_p A)}$.

Since the unit of σ_a is [m^2]. This is probably where the name of absorption cross-section comes from. As we mentioned above, it has nothing to do with the geometric cross section of the fiber. We also need to note that the absorption cross section does not mean attenuation, and it indicates the efficiency of energy conversion from photons to the excited carriers. Similarly, we can define an emission cross section

as: $\sigma_e = \frac{W_s}{(P_s / hf_s A)}$, where P_s and f_s are the emitted signal optical power and frequency, respectively. W_s is the stimulated emission efficiency, which is defined as the probability of each carrier in the metastable state that recombines to produce a photon within each second. It has to be emphasized that both absorption and emission cross sections are properties of the erbium doped fiber itself. They are independent of operation conditions of the fiber, such as pump and signal optical power levels.

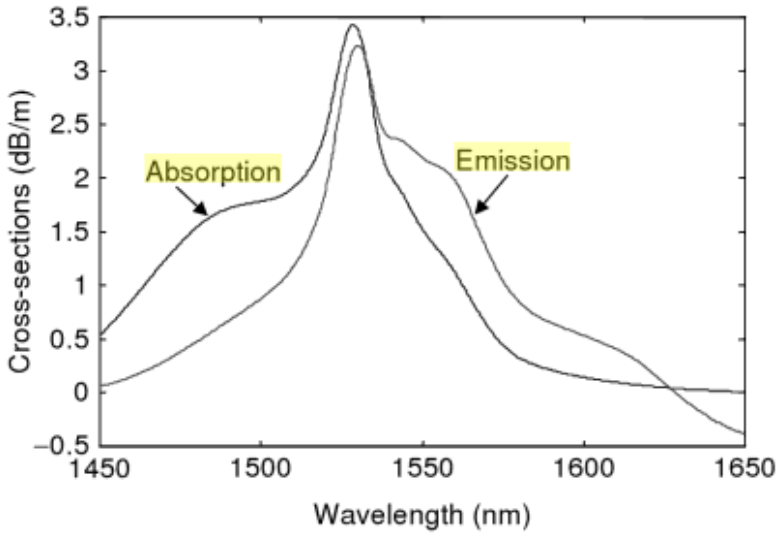

Figure 2-4 Absorption and emission cross section of HE980 erbium doped fiber, which are functions of wavelength.

At each wavelength both absorption and emission exist because photons can be absorbed to generate carriers through stimulated absorption process and at the same time new photons can be generated through stimulated emission process. Fig.2.4 shows an example of absorption and emission cross sections in an Er-doped silica optical fiber and obviously both of them are functions of wavelength.

If the carrier densities in the ground state and the metastable state are N_1 and N_2, respectively, the net stimulated emission rate per cubic meter is

$$R_e = W_s(\lambda_s)N_2 - W_p(\lambda_s)N_1 \tag{2.1}$$

where $W_s(\lambda_s)$ and $W_p(\lambda_p)$ are the emission and absorption efficiencies of the erbium doped fiber at the signal wavelength λ_s. Considering the definition of absorption and emission cross sections, this net emission rate can be expressed as

$$R_e = \frac{\Gamma_s \sigma_e(\lambda_s) P_s}{h f_s A}\left(N_2 - \frac{\sigma_a(\lambda_s)}{\sigma_e(\lambda_s)} N_1\right) \tag{2.2}$$

where a field confinement factor Γ_s is introduced to take into account the overlap factor between the signal optical field and the erbium doped area in the fiber core. The physical meaning of this net emission rate is the number of photons that are generated per second per cubic meter.

The rate equation for the carrier density in the metastable state N_2 is,

$$\frac{dN_2}{dt} = \frac{\Gamma_p \sigma_a(\lambda_p) P_p}{h f_p A} N_1 - \frac{\Gamma_s \sigma_e(\lambda_s) P_s}{h f_s A}\left(N_2 - \frac{\sigma_a(\lambda_s)}{\sigma_e(\lambda_s)} N_1\right) - \frac{N_2}{\tau} \tag{2.3}$$

On the right hand side of this equation, the first term is the contribution of carrier generation by stimulated absorption of the pump. The second term represents net stimulated recombination which consumes the upper level carrier density. The last term is spontaneous recombination, in which upper level carriers spontaneously recombine to generate spontaneous emission. τ is the spontaneous emission carrier lifetime. Because the emission cross section at the pump wavelength $\sigma_e(\lambda_p)$, is much smaller than the

absorption cross section at the signal wavelength $\sigma_a(\lambda_s)$, we neglected the mission term at pump wavelength for simplicity. In equation (2.1), both lower (N_1) and upper (N_2) state population densities are involved, however, these two carrier densities are not independent and they are related by

$$N_1+N_2=N_T \tag{2.4}$$

where N_T is the total erbium ion density that is doped into the fiber. The energy state of each erbium ion stays either in the ground level or in the metasable level. In the steady state (*d/dt*=0), if there are only one signal wavelength and one pump wavelength are involved, equation (2.3) can be easily solved with the help of equation (2.4),

$$N_2 = \frac{\Gamma_s\sigma_a(\lambda_s)f_pP_s + \Gamma_p\sigma_a(\lambda_p)f_sP_p}{\Gamma_p\sigma_a(\lambda_p)f_sP_p + \Gamma_s f_pP_s(\sigma_e(\lambda_s)+\sigma_a(\lambda_s)) + hf_s f_pA/\tau} N_T \tag{2.5}$$

Note that since the optical powers of both the pump and the signal change significantly along the fiber, the upper level carrier density is also a function of the location parameter z along the fiber $N_2=N_2(z)$. In order to find the z-dependent optical powers for the pump and the signal, propagation equations need to be established for them.

The propagation equations for the optical signal at the signal wavelength and at the pump wavelengths are,

$$\frac{dP_s(\lambda_s)}{dz} = g(z,\lambda_s)P_s(z) \tag{2.6}$$

where

$$g(z,\lambda_s) = \Gamma_s[\sigma_e(\lambda_s)N_2(z) - \sigma_a(\lambda_s)N_1(z)] \tag{2.7}$$

is the effective gain coefficient at the signal wavelength.

$$\frac{dP_p(\lambda_p)}{dz} = \alpha(z,\lambda_p)P_p(z) \quad (2.8)$$

where

$$\alpha(z,\lambda_p) = \Gamma_p\left[\sigma_e(\lambda_p)N_2(z) - \sigma_a(\lambda_p)N_1(z)\right] \quad (2.9)$$

is the effective absorption coefficient at the pump wavelength. We can easily understand these propagation equations by seeing it this way.

$$\sigma_e(\lambda_s)N_2(z)P_s(z) = W_s h f_s A N_2(z) \quad (2.10)$$

It is the optical power generated per unit length at the position z. Similarly,

$$\sigma_a(\lambda_s)N_1(z)P_s(z) = W_a h f_s A N_1(z) \quad (2.11)$$

is the optical power absorbed per unit length at position z. Note that the unit of both $g(z,\lambda_s)$ and $\alpha(z,\lambda_p)$ is in [m^{-1}].

The two propagation equations are mutually coupled through carrier density N_2 (z) and $N_1=N_T-N_2$ (z). Once the position dependent carrier density N_2 (z) is found, the performance of the EDFA will be known, and the overall signal optical gain of the amplifier can be found as.

$$G(\lambda_s, z) = \exp\left\{\Gamma\left[\left(\sigma_e(\lambda_s)+\sigma_a(\lambda_s)\right)\int_0^L N_2(z)dz - \sigma_a(\lambda_s)N_T L\right]\right\} \quad (2.12)$$

It depends on the accumulated carrier density along the fiber length.

2.3 Design Principles of Er doped waveguide

Thin film based integrated planar lightwave circuits (PLC) are becoming more and more important in photonics and optical communications. Passive PLC devices such as optical splitters, combiners, WDM multiplexers and demultiplexers, ring resonators and modulators are now commercially available. At the same time, Erbium dope planar optical waveguides, which can be integrated with these planar optical devices, are developed with the same concept of EDFA, which can be used as amplifiers for integrated photonic circuits such as PLC.

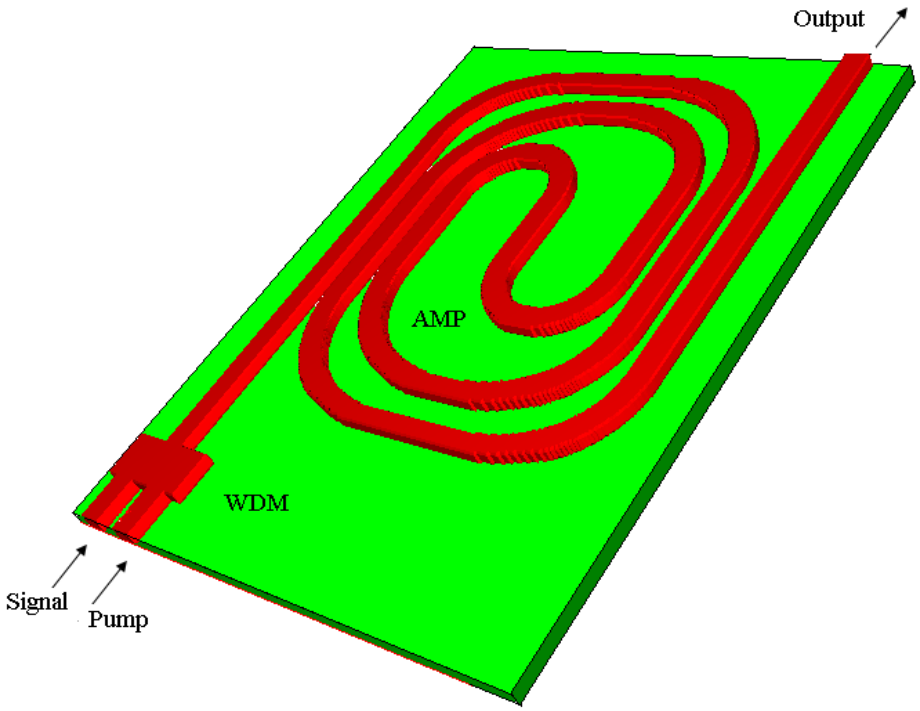

Figure 2-5 Example of an Er doped waveguide amplifier. The purpose of the curved structure is to reduce the size of the entire optical circuit

Figure 2-5 shows an example of PLC, which is also an Erbium doped waveguide amplifier. The 1550nm signal first enters a WDM (Wavelength Division Multiplexer) coupler, where it combines with an optical pump either at 1480nm or 980nm, which is used to excite Er^{3+} ions in AMP (the amplifier waveguide). The AMP is usually rolled up to reduce the size of the circuit. Optical waveguides exhibit additional propagation losses when they are bent. Typically, these losses rise very quickly once a certain critical bend radius R_c is reached. For a typical single mode optical fiber, the critical bend radius can be defined as [24]

$$R_c = \frac{3n_2\lambda}{4\pi(NA)^3},\ NA = \sqrt{n_1^2 - n_2^2} \qquad (2.13)$$

where n_1 is the refractive index of the core, and n_2 is the refractive index of clad. NA is the numerical aperture of the fiber. Therefore, a larger numerical aperture means a smaller critical bend radius. In order that signal can propagate along the curved waveguide, we must guarantee that the bending radius of curved waveguide is larger than its critical bend radius. So if we can achieve a big numerical aperture, the size of the whole curved waveguide will be greatly reduced. Compared with traditional silica waveguides, semiconductor waveguides with high refractive index contrast allow for very small integrated devices. The refractive index of III-V semiconductor GaN is about 2.33 at 1550nm wavelength, which is much higher than that of silica. So GaN based waveguide is one of the ideal candidates for compact integrated optical circuits.

Optical waveguide is a basic component which is essential in constructing complicated photonic devices in planar lightware circuits. There are many different

structures of planar optical waveguides. Figure 2.6 provides some examples of planar waveguides with different structures, including buried rectangular optical waveguides, slab optical waveguides and ridge optical waveguides.

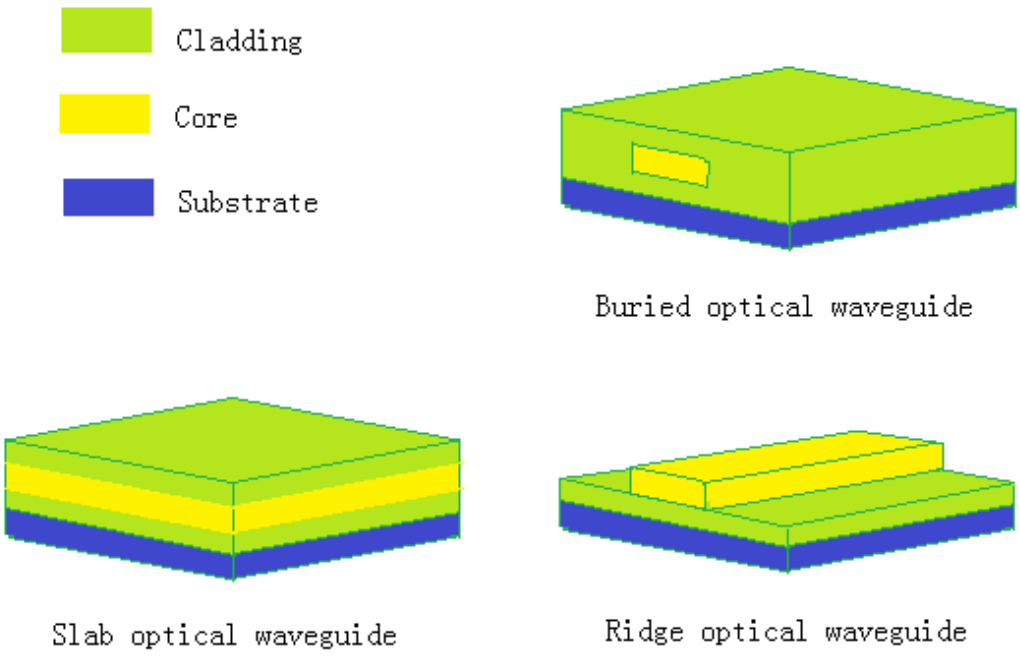

Figure 2-6 Example of Planar Optical Waveguide, which includes buried optical waveguide, slab optical waveguide and ridge optical waveguide

Actually, there are still many other structures that are not listed here, and the modeling method might be different for each structure. Analysis methods such as Marcatili's method and Effective index method were developed for straight rectangular dielectric waveguides. However, curvilinear directional couplers, branching and combining waveguides, S-shaped bent waveguides, and tapered waveguides are all indispensable components in constructing integrated optical circuits which cannot be modeled with

simple analytical techniques. So we need to use a more powerful method to deal with all these axial variations in waveguides.

Beam Propagation Method (BPM) works under slowly varying envelope approximation, for linear equations. BPM is a quick and easy method of solving for fields in integrated optical devices. It can be used to design single mode waveguides, to calculate the effective refractive index in the waveguide and to illustrate the transmission along a waveguide. Here we will briefly introduce the basic approach by formulating the problem under the restrictions of a scalar field and paraxiality.

The scalar field assumption allows the scalar electric field to be written as

$$E(x,y,z,t) = \phi(x,y,z)e^{-i\omega t} \tag{2.14}$$

So that the wave equation can be written in the form of the well-known Helmholtz equation for monochromatic waves:

$$\frac{\partial^2\phi}{\partial x^2} + \frac{\partial^2\phi}{\partial y^2} + \frac{\partial^2\phi}{\partial z^2} + k(x,y,z)^2\phi = 0 \tag{2.15}$$

Where $k(x,y,z) = k_0 n(x,y,z)$is the spatially dependent wavenumber, with $k_0 = \frac{2\pi}{\lambda}$ being the wavenumber in free space. The geometry of the problem is defined entirely by the refractive index distribution n(x, y, z). Considering that in typical guided wave problems, the most rapid variation in the field ϕ is the phase variation due to the propagation along the guiding axis (Z-direction in our analysis), it is beneficial to factor this rapid variation out of the problem by introducing a so called slowly varying field $\phi(x,y,z) = u(x,y,z)e^{i\bar{k}z}$ where $\bar{k}$ is the reference wavenumber, which is a constant

number to be chose to represent the average phase variation of the field ϕ. We can get the following equation by introducing the above expression into the Helmholtz equation.

$$\frac{\partial^2 u}{\partial z^2}+\frac{\partial^2 u}{\partial x^2}+\frac{\partial^2 u}{\partial y^2}+2i\bar{k}\frac{\partial u}{\partial z}+\left(k^2-\bar{k}^2\right)u=0 \qquad (2.16)$$

If we assume that the variation of $u(x,y,z)$ with z is sufficiently slow, the term $\frac{\partial^2 u}{\partial z^2}$ can be neglected with respect to the term $2i\bar{k}\frac{\partial u}{\partial z}$. This assumption is called the paraxial or parabolic approximation.

BPM can be developed based on the finite difference method (FDM). In the finite-difference approach, the field in the transverse XY plane is represented only at discrete points on a grid, and at discrete planes along the longitudinal or propagation direction Z. Given the discretized field at one z plane, the goal is to derive numerical equations that determine the field at the next z plane. This elementary propagation step is then repeated to determine the field throughout the structure.

For simplicity, the approach is illustrated for a 2D scalar field, which works well for the lightwave propagation in slab waveguides, and the two dimensional scalar wave equation should be like this

$$\frac{\partial u}{\partial z} = \frac{i}{2\bar{k}}\left[\frac{\partial^2 u}{\partial x^2} + \left(k^2 - \bar{k}^2\right)u\right] \tag{2.17}$$

Let u_i^n denote the field at transverse grid point i and longitudinal plane n, and assume the grid points and planes are equally spaced by Δx and Δz apart, respectively. Then the above differential equation can be approximated by the finite difference method as

$$\frac{u_i^{n+1} - u_i^n}{\Delta z} = \frac{i}{2\bar{k}}\left[\frac{\delta^2}{\Delta x^2} + \left(k\left(x_i, z_{n+1/2}\right)^2 - \bar{k}^2\right)\right]\frac{u_i^{n+1} + u_i^n}{2} \tag{2.18}$$

δ^2 represents the standard second order difference operator, $\delta^2 u_i = u_{i+1} + u_{i-1} - 2u_i$, and $z_{n+1/2} \equiv z_n + \Delta z/2$ The above equation can be rearranged into the form of standard tridiagonal matrix equation for the unknown field u_i^{n+1} in terms of known quantities, resulting in

$$a_i u_{i-1}^{n+1} + b_i u_i^{n+1} + c_i u_{i+1}^{n+1} = d_i \tag{2.19}$$

The tridiagonal nature of the above equation allows rapid solution in order O(N) operations, where N is the grid points in X [25]. A commonly used boundary condition is the so-called transparent boundary condition or TBC. The basic approach is to assume that near the boundary the field behaves as an outgoing plane wave, with characteristics (amplitude, direction) that are dynamically determined via some heuristic algorithm. The plane wave assumption allows the field at the boundary point to be related to the adjacent interior point, thus completing the set of equations. The TBC is generally very effective

in allowing radiation to freely escape the computational domain. It should be noted that the paraxial approximation has been adopted in the above FDM analysis. Therefore, this method is not very good for analyzing light beam propagation in a highly tilted waveguide from the initial propagation direction of the input signal.

2.4 Excitation dynamics of the 1.54um emission in Er doped GaN

For an Erbium doped photonic device, although the solid host does not affect the wavelength of the emission, the transition probability is affected by the neighboring environment of the erbium ions. The fact that Erbium emission from semiconductors of smaller band gaps has low efficiency at room temperature due to a strong thermal quenching has been empirically determined. The empirical work by *Favennec et al* [26] has directed researchers to use wide band gap semiconductors (WBGS) as host materials for Erbium. The following table shows the band-gaps of several materials at room temperature (about 300K).

Table 2-1

Materials	InN	Si	GaAs	GaN	SiO_2
Bandgap	0.65 eV	1.12 eV	1.424 eV	3.4 eV	8.9 eV

In Table 2-1, GaN is the semiconductor material with the largest bandgap (SiO2 is not a semiconductor), which has proven to be an accomplished host of erbium, with reports of fabrication of light-emitting diodes operating in the visible and infrared region[15]. However, since these devices suffer from low quantum efficiency at the IR wavelength, it is very important to have a better understanding of the excitation and

emission dynamics of the Er doped GaN system, so we can create materials suitable for telecommunication applications.

Some reports [10] have associated the mechanisms of this thermal quenching with an Er related trap energy level located within the energy band gap. Through this Er trap, the 4f core states are excited by an Auger energy transfer via bound carriers. When the environment temperature is high, the thermal energy of the surrounding environment becomes large enough to make the carriers dissociated from the Er center, so that the energy transfer efficiency drops dramatically, thus resulting in the thermal quenching of transition efficiency.

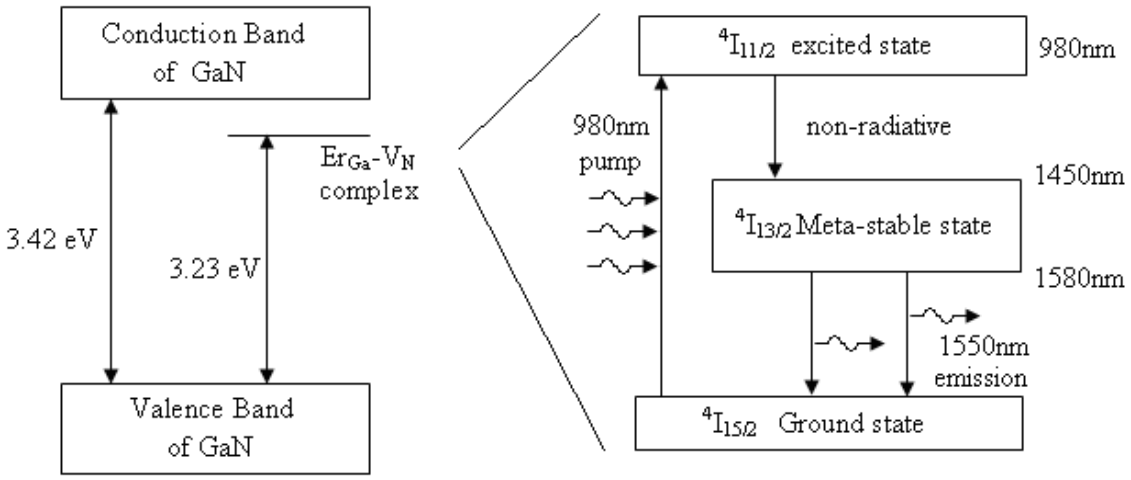

Figure 2-7 Simplified Energy band structure of Er:GaN, and the relationship between the energy band structure of Erbium and band structure of the semiconductor host

Unlike Erbium doped in Silica, the interaction between Er ions and semiconductor lattice structure of GaN introduced the Er_{Ga}-V_N complex, which results in an Er trap-related donor level. Fig.2.7 shows the energy band structure of Er doped GaN, from which we can see a half filled energy level at approximately 0.2eV below the conduction band of GaN.

Fig.2-8 shows the experimental data provided by researchers from Texas Tech University [10]. In Fig.2.8 (a), the dominant band edge emission of undoped and Er doped GaN at 10 and 300K are compared in detail for 263nm excitation. The dominant band edge emission of Er doped GaN is 3.23eV, which is 0.19eV smaller than the dominant band edge emission of undoped GaN at a room temperature. The inset of Fig.2.8 (a) is the temporal response of the 3.23eV PL emission peak in Er doped GaN measured at 10K. The lifetime of the 3.23eV transition was determined to be 200ps, which suggests that this is an impurity-to-band related transition.

Fig.2.8 (b) is a plot of the integrated PL emission intensity (I_{int}) of the 1.54um emission from Er doped GaN between 10 and 450K for 263nm excitation. The Er emission has a 20% decrease in $\boldsymbol{I_{int}}$ between 10K and 300K, which represents the lowest reported degree of thermal quenching for rare earth doped GaN. The data from Fig.2.8 (b) were fitted by the equation $I_{\text{int}} = \frac{I_0}{1+ce^{-E_0/kT}}$, where I_0 is the integrated intensity at low temperature, c is a fitting constant, E_0 is the activation energy of the thermal quenching, and k is the Boltzmann's constant. The inset in Fig.2.8 (b) is an Arrhenius plot of the integrated PL emission intensity at 1.54um between 10 and 450K. From this

plot, an activation energy of 191meV was determined, which coincides with the 0.19eV difference in Fig.2.8 (a).

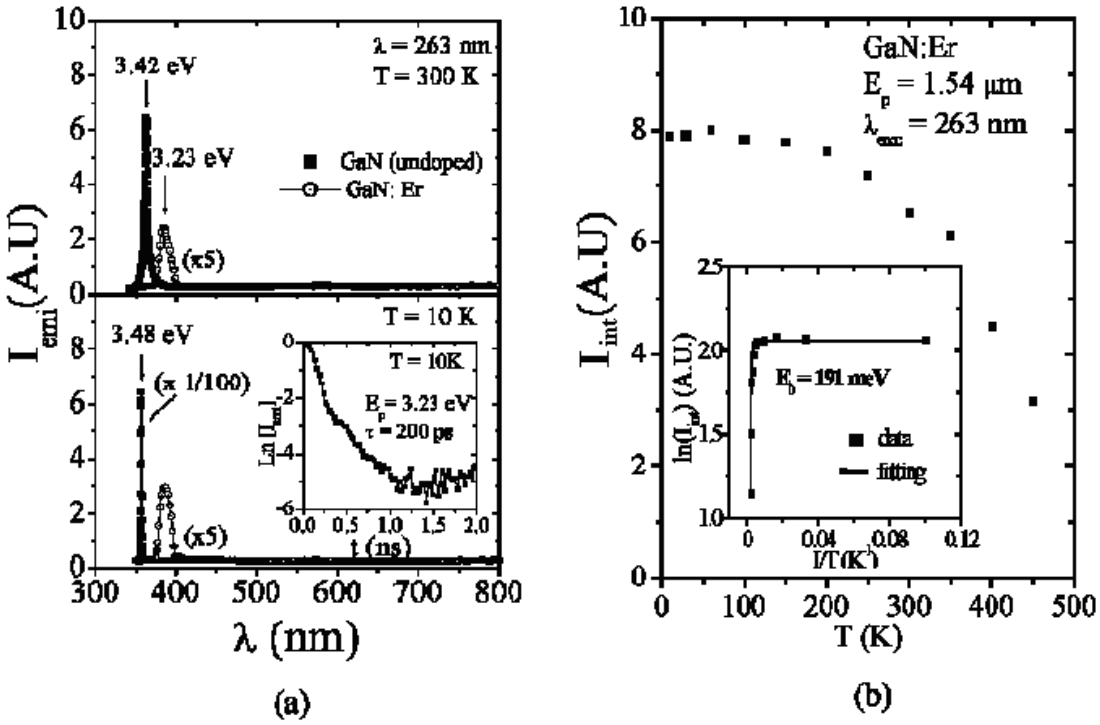

Figure 2-8 Experimental data for band edge emission, which was measured by Texas Tech University [10]

Thus, the dominant 3.23eV band edge PL emission in Er doped GaN was believed to be due to the recombination between electrons bound to the Er_{Ga}-V_N complex and free holes in the valence band, and the exchange of energy between the electrons bound to the Er_{Ga}-V_N complex and the 4f core states of Er was the dominant excitation mechanism of the 1.54um emission using the above band gap excitation [10].

These results provide a better understanding of the low degree of thermal quenching in WBGS. It is well established that for semiconductors, effective donor levels

increase with increasing energy band gap. This can explain the low degree of thermal quenching for Er doped WBGS.

For Er doped in smaller band gap semiconductors, it is relatively easier for the majority of electrons bound to the Er trap to be excited into the conduction band since the binding energy is small, and that is why smaller band gap semiconductors suffer from a higher thermal quenching. In the contrary, for WBGS, only in a high temperature environment, will be thermal energy big enough to excite majority of electrons bound to the Er trap into the conduction band, so that the Auger energy transfer between bound electrons and 4f electrons can still occur at even a high temperature and the subsequent thermal quenching is dramatically reduced.

2.5 Absorption and Emission Cross Section Measurement

Absorption and emission cross sections (CS) are two important parameters related with the doping ion and material host characteristics, which can greatly affect the performance of rare earth ions in solid state laser media.

Usually, absorption cross section is measured first, and the emission cross sections can be calculated from the absorption cross section. For the characterization of integrated waveguides like our Er:GaN device, the wavelength dependent absorption cross section is evaluated from the measured absorption spectrum from homogeneously doped waveguide samples with a known erbium concentration. In this process, prior knowledge of the mode-normalized intensity distribution, the erbium concentration distribution, as well as the scattering and insertion losses is required. In addition, a relatively powerful light source is needed in order to permit a direct measurement of attenuation spectrum, because erbium doped integrated waveguides usually present high insertion and scattering losses [17-23].

Then a basic form of Füchtbauer–Ladenburg (FL) equation is used to relate emission cross section to absorption cross section.

$$d_1 \int \nu^2 \sigma_a(\nu) d\nu = d_2 \int \nu^2 \sigma_e(\nu) d\nu \qquad (2.20)$$

Where d_i is the degeneracy of level i, ν is the photon frequency, and σ_a and σ_e are the absorption and emission cross sections. This relationship holds for rare earth ions only when all sub-levels of each energy state are equally populated, or all the transitions have the same rate. However, the emission spectral bandwidth of Er doped GaN is about

300cm^{-1}, which is quite different from kT=200cm^{-1}(at room temperature). In addition, the transition strength is sensitive to the Stark levels involved according to low temperature absorption and emission measurements. Therefore, the above condition is not satisfied for Er:GaN at room temperature due to different populations of the sub-levels of each state.

In the contrary, emission spectra measurements do not require such wideband tunable and high power source, and fewer parameters are needed when we want to determine emission cross section from the measured spontaneous emission spectrum. Therefore, if the absorption cross section could be determined from the emission cross section, the process would be less susceptible to experimental uncertainties. Moreover, in order to get the relationship between absorption and emission cross sections, a general form of McCumber's theory has to be used. The only requirement for the theory of McCumber is that the time necessary to establish a thermal distribution with each manifold should be shorter compared to the lifetime of that manifold. According to McCumber's theory, the absorption and emission cross sections can be related by

$$\sigma_e(\nu) = \sigma_a(\nu)\exp\left(\frac{h\nu - \varepsilon}{kT}\right) \tag{2.21}$$

where ε is the temperature dependent excitation energy, which is the net energy needed to excite an Er^{3+} ion from the $^4I_{15/2}$ to the $^4I_{13/2}$ state at temperature T. The above equation indicates that frequency $\nu_c \equiv \varepsilon/h$ is the only intersection frequency between the two cross section curves σ_a and σ_e.

σ_e is smaller than σ_a at frequencies higher than ν_c and vice versa for $\nu < \nu_c$. The excitation energy ε can also be evaluated using an alternative definition

$$\frac{N_2}{N_1} = \exp\left(\frac{-\varepsilon}{kT}\right) \tag{2.22}$$

where N_2 and N_1 represent thermal equilibrium populations of the 1st excited state (or the metastable state in Fig.2-2) and the ground state, respectively, without any pump. If the accurate information for all the state's Stark components is known, N_2/N_1 can be evaluated by the following equation,

$$\frac{N_2}{N_1} = \exp\left(\frac{-\Delta E_{21}}{kT}\right)\frac{1+\sum_{i=2}^{d_2}\exp\left(-\delta E_{2i}/kT\right)}{1+\sum_{i=2}^{d_1}\exp\left(-\delta E_{1i}/kT\right)} \tag{2.23}$$

where ΔE_{21} represents the separation between the lowest sub-level of the 1st excited state and the lowest sub-level of the ground state , δE_{2i} is the energy difference between the *i*th and the lowest component of the 1st excited state, while δE_{1i} is energy difference between the *i*th and the lowest component of the ground state. With a proper assumption to simplify the electron structure, ε can be determined by substituting (2.22) into (2.32), and the absorption cross section is related to emission cross section by McCumber theory as shown in (2.21).

In practice, emission spectrum is usually easier to measure than the absorption spectrum, especially for short waveguides where the erbium absorption is too low to measure accurately. So that we chose to determine the emission cross section first, and then derive the absorption cross section based on the McCumber's theory. In fact, if the radiative carrier lifetime can be precisely measured, one can derive the emission cross section through the Füchtbauer–Ladenburg (FL) equation,

$$\frac{1}{\tau_e} = \frac{8\pi n^2}{c^2}\int \nu^2 \sigma_e(\nu) d\nu = 8\pi n^2 c \int \frac{\sigma_e(\lambda)}{\lambda^4} d\lambda \tag{2.24}$$

where τ_e is the radiative carrier lifetime of the 1st excited state, n is the refractive index of the solid host, c is the light velocity in vacuum, and σ_e denotes the wavelength-dependent emission cross section. Within a narrow frequency band, the emission cross section in the FL equation is proportional to the spontaneous emission intensity $I(\lambda)$ which can be directly measured, and therefore Eq(2.24) can be rewritten as

$$\sigma_e(\lambda) = \frac{\bar{\lambda}^4}{8\pi c n^2 \tau} \frac{I(\lambda)}{\int I(\lambda) d\lambda} \tag{2.25}$$

Where $\bar{\lambda}$ is the average wavelength of the measured spontaneous emission spectrum. Equation (2.25) shows that the emission cross section can be obtained from the carrier lifetime and the normalized emission spectrum, while the absolute power density values of the spontaneous emission are not important.

EXPERIMENTAL TECHNIQUES

3.1 Sample Information and Experiment Setup

The Er-doped GaN epilayers used in this work were synthesized by metal organic chemical vapor deposition (MOCVD) in a horizontal reactor. Trimethylgallium was used for the Ga source, and blue NH_3 was used as the N source. The metal organic precursor used for the *in situ* Er doping was tris (2,2,6,6-tetramethyl-3,5-heptanedionato) erbium, which was transported to the reactor by H_2. All samples were grown on (0001) sapphire substrates. The growth of these epilayers began with a thin (~30nm) GaN buffer layer, followed by a 1.4um GaN epilayer template and a 0.5um Er-doped GaN layer. The growth temperature of the GaN template and Er-doped GaN layer was 1040 C.

The waveguides were fabricated on the Er-doped GaN epilayers using optical lithography and inductively coupled plasma dry etching. A 250nm SiO_2 passivation layer was deposited on top of the waveguides by plasma enhanced CVD to reduce the optical scattering. The layered structure of the waveguide is shown in Fig.1 which is about 5um wide and 2.6mm long. The 0.5um thick Er-doped GaN layer has an Er concentration of approximately $5\times10^{20}cm^{-3}$.

Figure 3.1 shows the cross section of our Er:GaN waveguide with layered structure. The refractive index of the 0.5um thick Er:GaN layer is n=2.335, and the refractive index of the 1.4um GaN layer is n=2.313, which was provided by our collaborators from Texas Tech University. A numerical calculation using beam propagation method (BPM) software was performed for this structure.

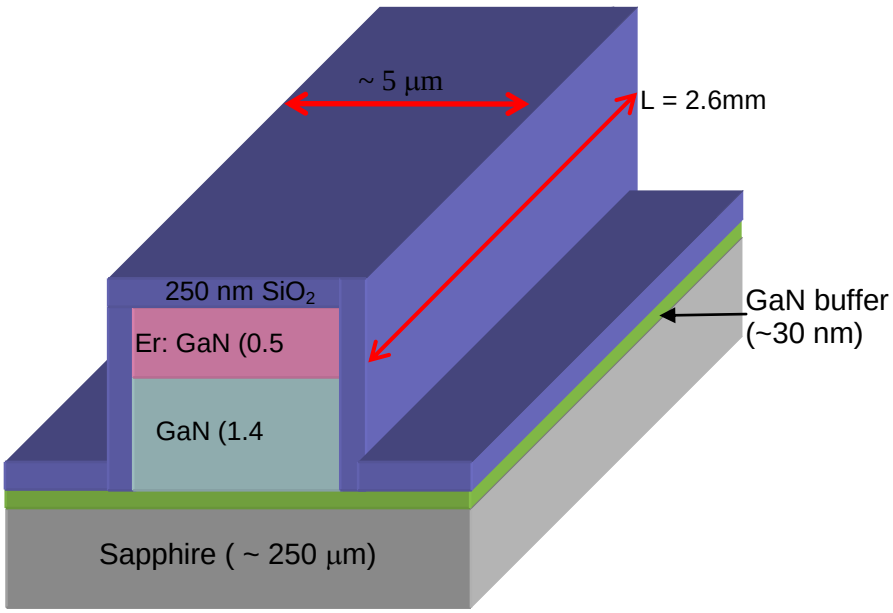

Figure 3-1 Layered structure of the Er-doped GaN waveguide. The pink color area shows the Erbium doped layer.

During the simulation, a Gaussian beam was used as the launched excitation, so that the mode could quickly converge to a stable solution. Figure 3.2 shows the fundamental mode profile calculated with BPM based on the above parameters.

However, the GaN layer doped with Erbium is only 0.5um thick, so that only a relatively small portion of the fundamental mode power is overlapped with the Er doped layer, which might be amplified when pump power is added. As we can see from Figure 3-2 (a), the mode field is the strongest at the position where Y=1.0um, so that it is important to determine quantitatively how much power of the mode is overlapped with the Er doped layer.

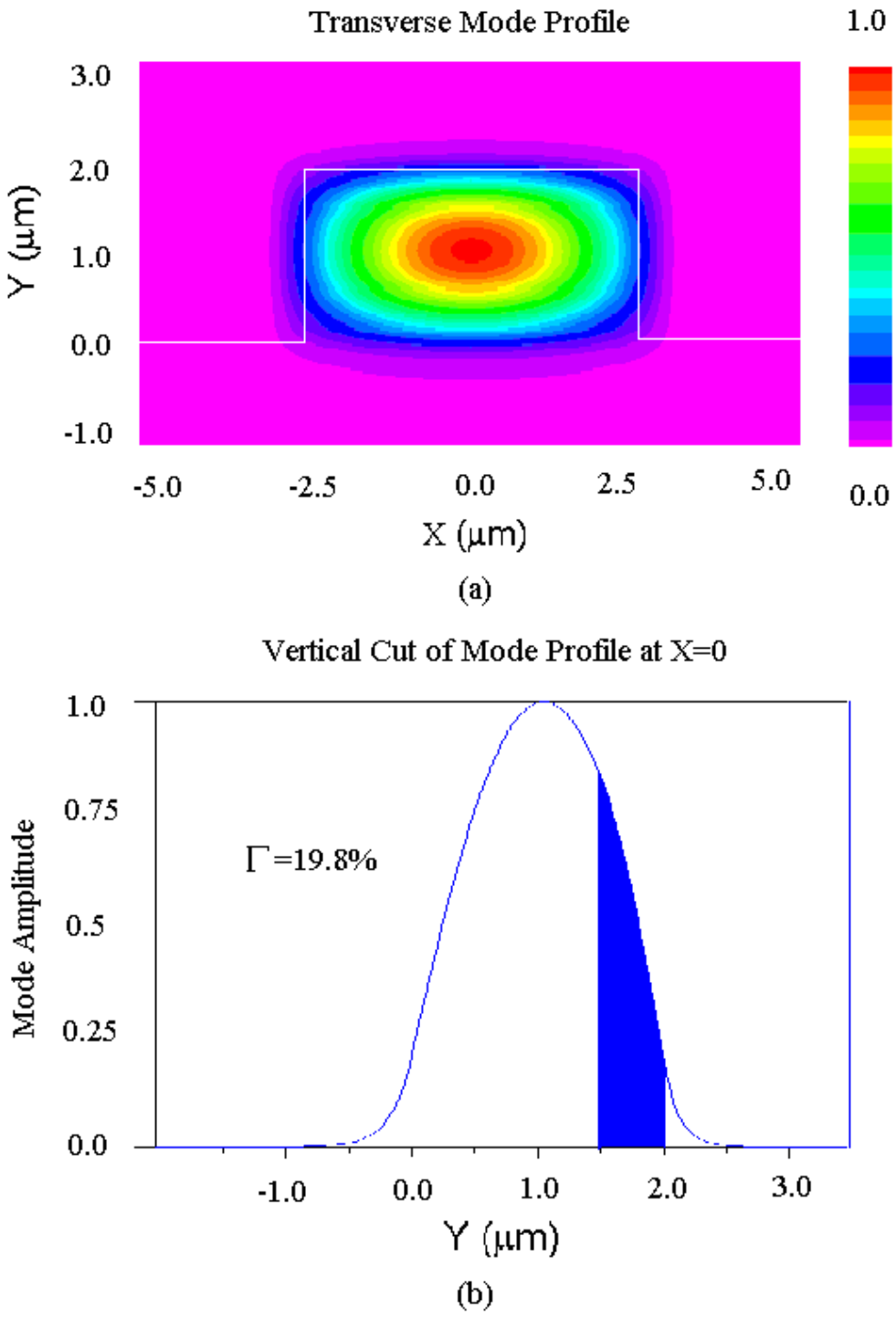

Figure 3-2 Transverse Mode Profile calculated by BPM (a), and Confinement factor (b). Fig (b) is the vertical cut of the Fig (a) at the position X=0.

Confinement factor, which is also called the "overlap factor", is a very important parameter when characterizing the performance of an optical amplifier. Because it is difficult to measure the confinement factor directly, numerical simulation will have to be used providing that the detailed information about the waveguide is known. Figure 3.2(b) highlights the overlap between the mode field profile and the Er-doped layer, which indicates that the confinement factor is approximately 19.8%.

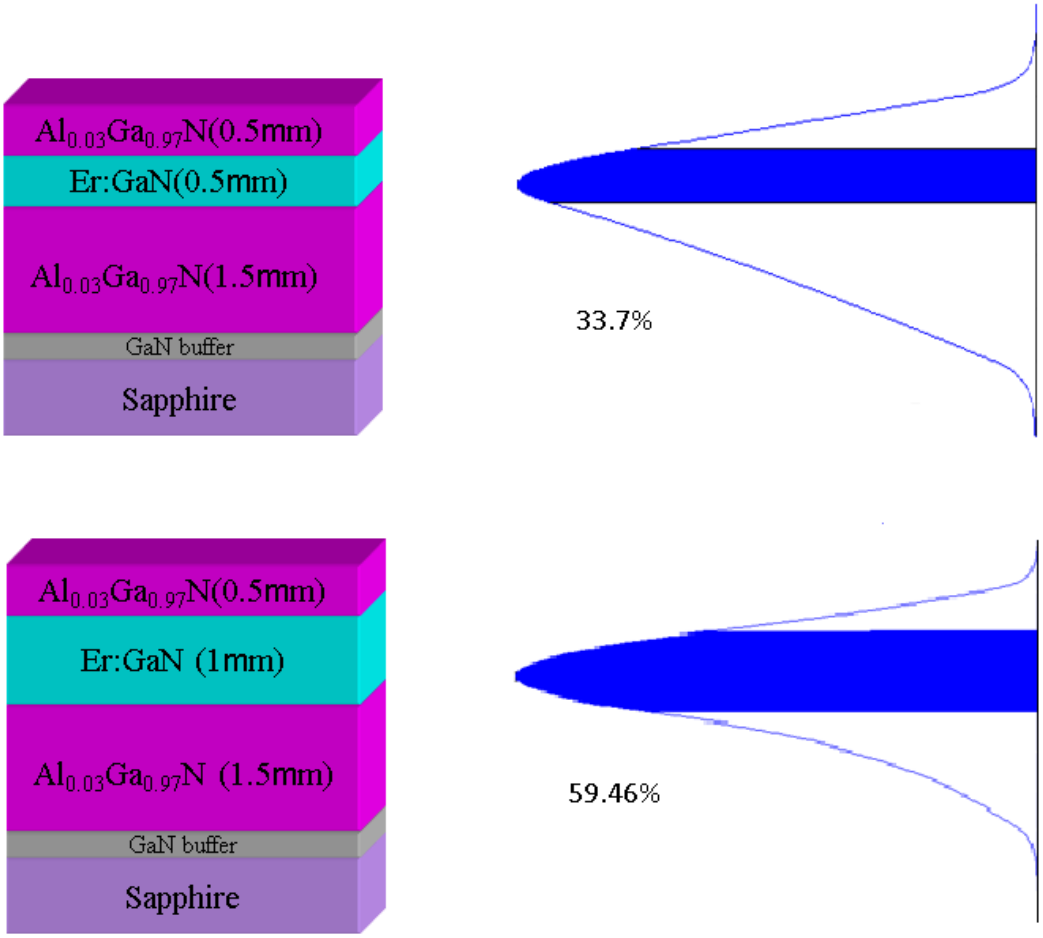

Figure 3-3 Other waveguide structures which can increase the confinement factor, either by moving the fundamental mode higher or by increasing the thickness of the Erbium doped layer.

Fig.3-3 shows two other waveguide structures with improved confinement factors in comparison to the waveguide shown in Fig3-1. In the first design in Fig.3-3, we added an extra AlGaN layer on top of the Er doped layer, which made the center of the fundamental mode move to a higher position, so that the peak position of the mode overlaps the Er doped layer. In the second design in Fig.3-3, the thickness of Er doped layer is increased so that the confinement factor can be further increase to approximately 60%. These two designs shown in Fig.3-3 can be used to improve the performance of the Er doped waveguide in the future, but we only used the original waveguide in our experiment.

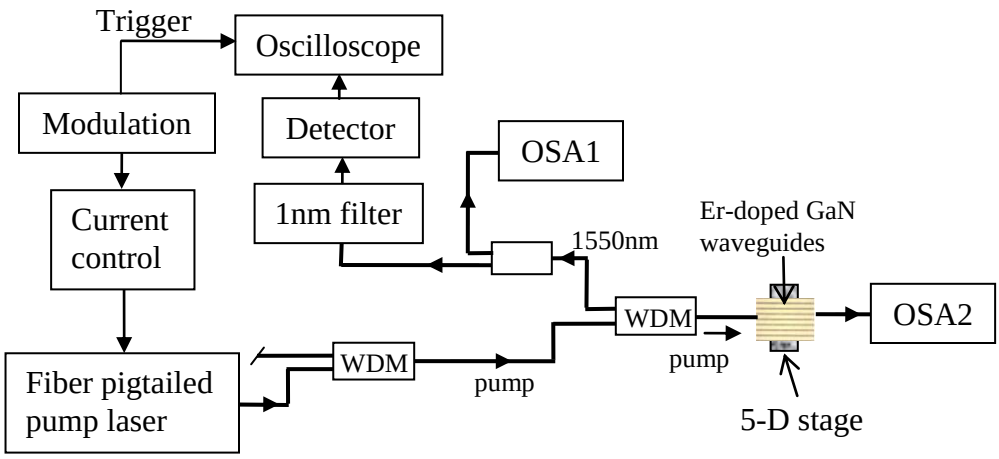

Figure 3-4 Experimental setup for our measurement

The experimental setup is shown in Figure 3.3. A fiber pigtailed laser diode, either at 980 or at 1480nm wavelength, is coupled into the Er doped GaN waveguide through two WDM fiber couplers which provide more than 40dB isolation between the 1480nm (980nm) and 1550nm wavelength bands. A single mode fiber with a tapered tip

was used to guide and focus the 1480nm (or 980nm) optical pump into the Er-doped GaN waveguide. The same fiber tip also collects the counter-propagating 1540nm spontaneous emission generated from the waveguide and sends it to an optical spectrum analyzer (OSA1) for measurement. The spontaneous emission at 1537nm was also selected by a bandpass optical filter for power measurement, and the time domain modulation response can also be measured.

During the experiment, two kinds of pump lasers were used. One is the LU0980M430, which can provide up to 430mW power at wavelength ranging from 970nm to 985nm. The other laser is FOL1404QNJ manufactured by Fitel, which can provide up to 250mW output power at 1480nm wavelength. For the purpose of temperature and driving current control, we chose to use LDTC2/2 produced by Wavelength Electronics in our laser system. LDTC2/2 combines WTC3243 (a 2.2 Amp laser driver) and WLD3343 (a 2.2 Amp temperature controller) on one small board so that it is available as an open frame in a chassis mount enclosure. In addition, the rise time and fall time of the maximum output driving current for WLD3343 is 160ns and 320ns, respectively, so that the output power of the pump laser can be modulated.

A high responsivity InGaAs photodiode/receiver operated with a thermoelectric cooler for thermal noise reduction was used to detect the spontaneous emission from the pumped optical waveguide. Since the bandwidth of our InGaAs photodiode is over 1 kHz, it should be enough to be used for the measurement of a carrier lifetime around several milliseconds.

The oscilloscope in our system is LeCroy WAVEMASTER 8600A, which is a real time digital oscilloscope with a long memory, and its sampling speed is up to 20GS/s corresponding to 6GHz analog bandwidth on all 4 channels.

3.2 Experimental Results and Data Analysis for Carrier lifetime

In this section we will present the results obtained from Photoluminescence (PL) measurements of Er doped GaN waveguide samples, as well as the carrier lifetime at room temperature. Figure 3.4 shows the measured spontaneous emission spectra when the waveguide was excited by 1480 and 980nm optical pumping.

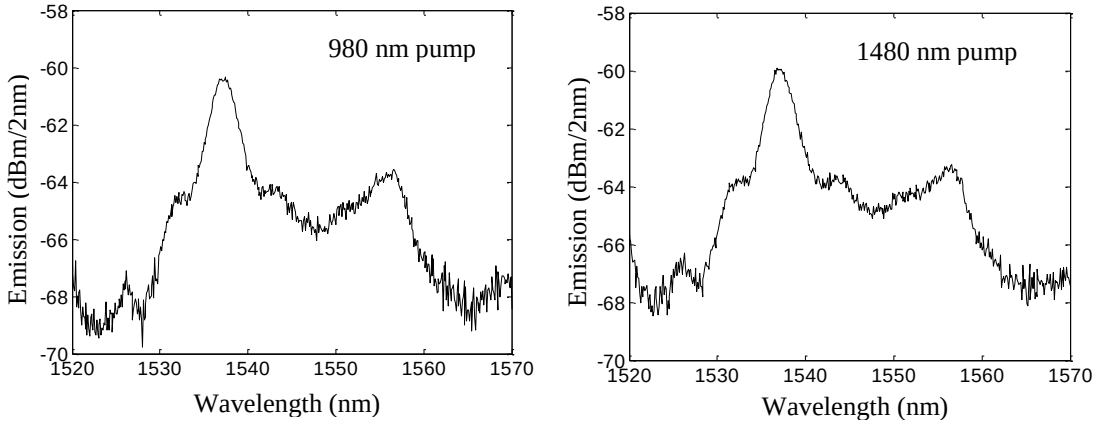

Figure 3-5 Measured spontaneous emission spectra in 1540nm window with 50mW pump at 980nm (a) and 80mW pump at 1480nm (b)

Comparing Fig.3-5 (a) and (b), it is evident that the shape of the emission spectra did not change with different pump wavelengths. In both cases, the emission covers approximately 30nm optical bandwidth, which is comparable to that in Er doped silica. When the pump power is high enough to achieve the highest carrier inversion between $^4I_{13/2}$ and $^4I_{15/2}$ energy levels, the peak emission density at 1537nm reached to

approximately -60 dBm for the resolution bandwidth of 2nm with either pumping source. This was obtained with the waveguide with 2.6mm in length.

In order to evaluate the dynamic response we passed the spontaneous emission through a 1nm bandpass optical filter at 1537nm and used an InGaAs photodiode to detect the optical power, and the waveforms were recorded by our real time oscilloscope. By suddenly switching off the 1480nm pump laser, the decay rate of the photoluminescence in 1537nm is determined by the carrier lifetime on the $^4I_{13/2}$ energy level. The measured falling edge of the spontaneous emission after switching off the pump shown in Figure3.6 exhibits a fast time constant of 1.5 ms and a slower time constant of 2.8ms.

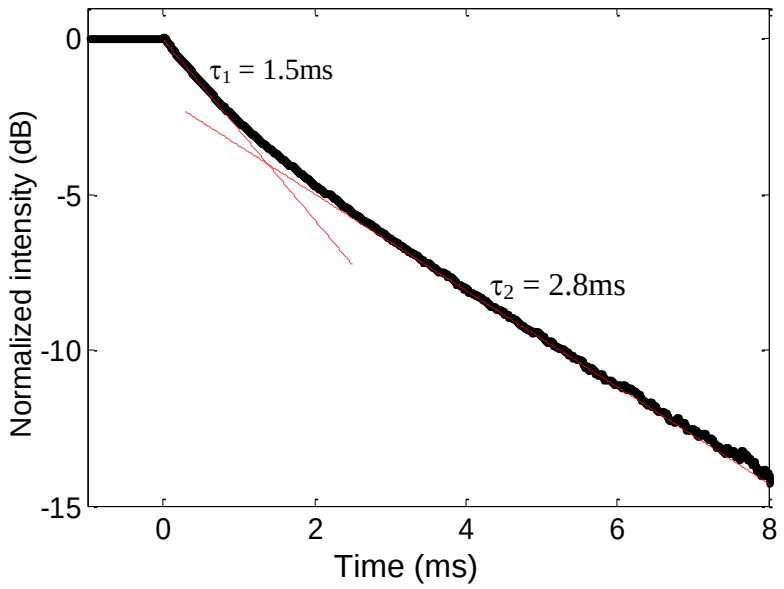

Figure 3-6 Falling edge of the measured spontaneous emission at 1537nm wavelength after the 1480nm pump laser was switched off at t=0

Considering an approximately -4dB optical loss including the coupling loss from the waveguide to the fiber (3 dB) and the loss of the WDM coupler (1dB), the actual power spectral density emitted from the waveguide at 1537nm should be approximately -56 dBm/2nm. This spontaneous emission power spectral density can be calculated by

$$\rho_{ASE} = 2\Gamma\sigma_e(\lambda_s)h\nu_s\int_0^L \frac{N_T P_p e^{-2\alpha z}\sigma_a(\lambda_p)}{P_p e^{-\alpha z}\left[\sigma_a(\lambda_p)+\sigma_e(\lambda_p)\right]+h\nu_p A/\tau}dz \qquad (3.1)$$

Where, σ_e and σ_a are emission and absorption cross sections and N_T is the doping density of erbium ions. λ_p is the pump wavelength, λ_s is the carrier lifetime, Γ is the field confinement factor, L is the length of the waveguide, $h\nu_s$ is the signal photon energy, A is the waveguide cross section, α is the attenuation, and $P(\lambda_p)$ is the pump optical power. For such a short waveguide, we have neglected the saturation effect caused by spontaneous emission in the 1540 nm wavelength to simplify the calculation. Using the cross section values of erbium doped in silica glass and the pump wavelength at λ_p=1480nm, $\sigma_a(\lambda_p)=1\times10^{-21}cm^2$, $\sigma_e(\lambda_p)=0.5\times10^{-21}cm^2$ and $\sigma_e(\lambda_s)=5\times10^{-21}cm^2$, and assuming the doping density of $N_T=5\times10^{20}cm^{-3}$, carrier lifetime $\tau=1.5ms$ (the longer time constant 2.8ms is only responsible for the radiative recombination, while the shorter time constant 1.5ms is the total carrier lifetime involing nonradiative components), and waveguide length L = 2.6 mm, the emission power spectral density can be calculated at 1537 nm wavelength as the function of pump power, as shown in Fig.3.7.

We have also assumed the attenuation of the waveguide of 1.5dB/mm. With 50mW pump power, the theoretical power spectral density emitted from the waveguide is

-55dBm/2nm, which is about 1dB higher than the measured value. This reduced efficiency is attributed to the non-radiative recombination and Auger recombination for the transition from the metastable level ($^4I_{13/2}$) to the ground level ($^4I_{15/2}$).

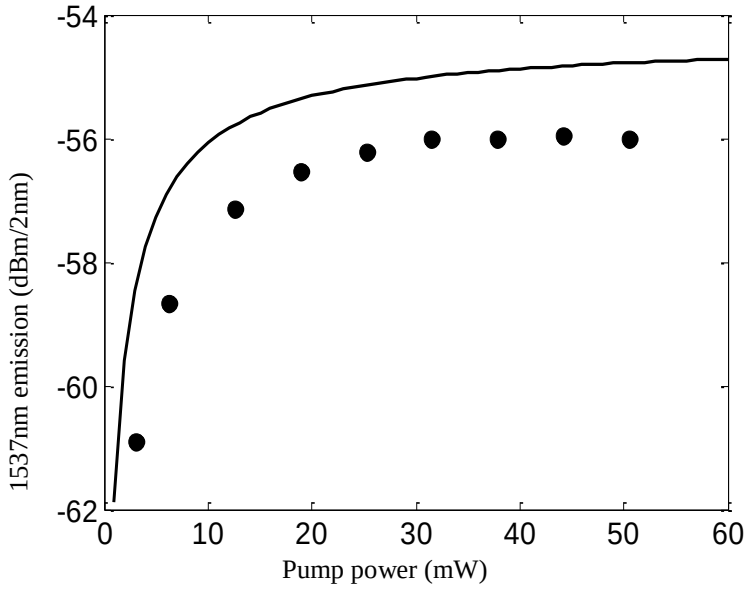

Figure 3-7 Calculated (continuous line) and measured (dots) spontaneous emission power spectral densities at 1537nm wavelength as functions of injected power of 1480nm pump laser.

Noting that although σ_a and σ_e values borrowed from erbium doped silica may not be quantitatively accurate for GaN, the calculated result shown in Figure 3.7 qualitatively agrees with the measurement, which provides a reasonable estimation of the pump efficiency.

During our experiment, we not only demonstrated a non-exponential decay curve (with two time constants), but also observed strong visible green light emitted from the pumped waveguide which is strong enough to be seen with bare eyes. The non-

exponential decay indicated the existence of Auger recombination and cooperative up-conversion which is responsible for exciting carriers to higher energy levels. Figure.3.8 shows the measured emission spectrum in the 400—1100nm wavelength window using a charge coupled device based optical spectrometer which is OSA2 in Figure3.3.

Although the waveguide was excited by a 1480nm pump, spectral components shown in Figure.3.8 include the recombination from all the higher energy levels of Er-ion up to the $^2H_{11/2}$. This energy up-conversion is attributed to the interaction between the doped Er-ions and the semiconductor lattice structure, and it is responsible for the green light generation in the pumped waveguide.

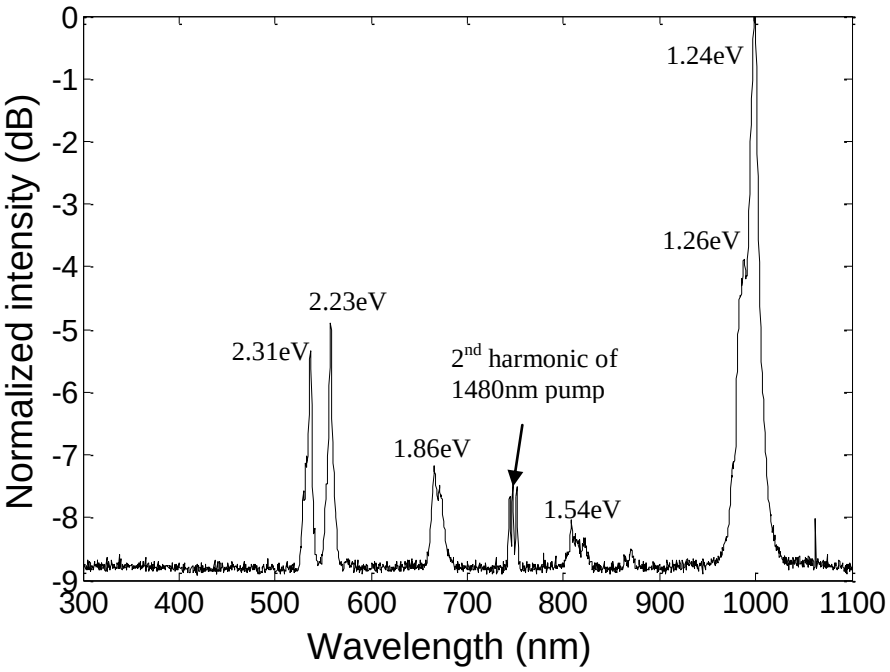

Figure 3-8 Room temperature emission spectrum of Er:GaN waveguide in the short wavelength region with 1480nm pumping laser.

The emission at the wavelength of 747nm is the 2nd harmonic of our 1480 nm pump, and the other emission peaks correspond well with the Erbium inner shell transition energy levels, which are illustrated in Figure.2.2.

Up-conversion can be observed only when the pump intensity is high enough to maintain a high concentration of excited Er ions. It is a very important effect in planar amplifiers, and it is a limiting factor of optical gain and amplifier efficiency, because a certain amount of pump energy is wasted for the emission in the visible light region.

3.3 Calculation of transition cross sections

In this thesis section, we will calculate the emission cross section from the measured spontaneous emission spectrum, and then apply the McCumber's theory to obtain the absorption cross section. Because we need wider range of emission spectrum that covers 1480 nm pump wavelength, while the strength of the spontaneous emission from a short Er:GaN waveguide is very weak especially in the wavelength region shorter than 1500nm, an optical spectrum analyzer with higher Signal to Noise ratio (SNR) at short waveguide is needed.

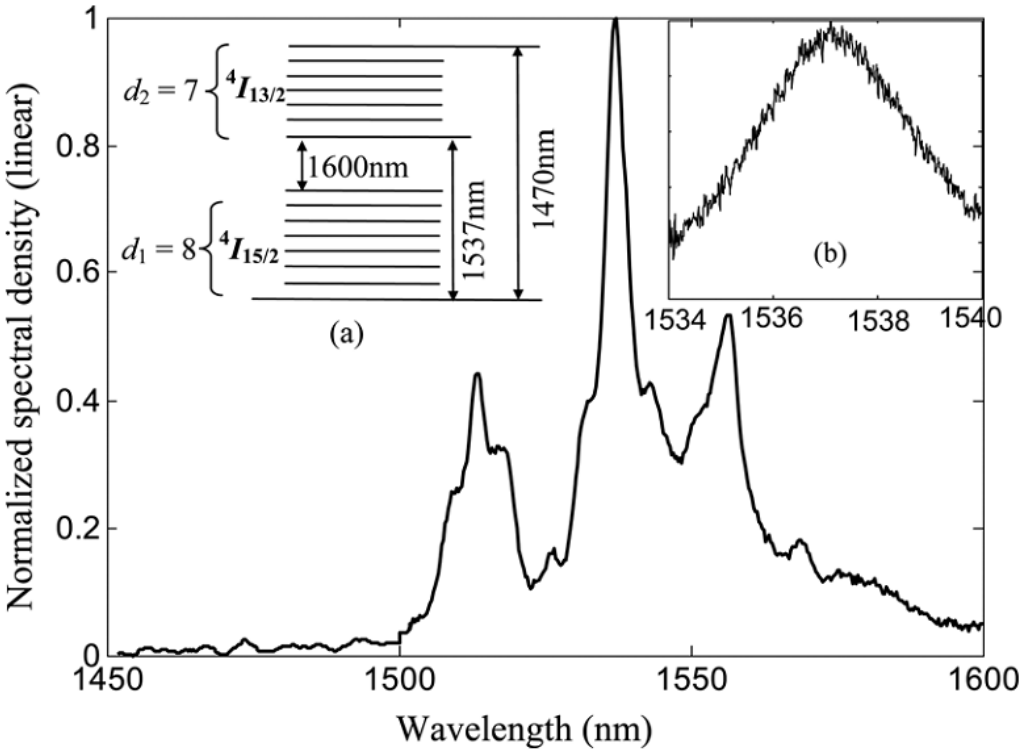

Figure 3-9 Normalized emission spectrum of a Er:GaN waveguide measured by an OSA with 2 nm resolution. Inset (a): detailed band diagram of erbium ions in the 1st excited band and the ground state. Inset (b): detailed emission spectrum measured near 1537 nm with 0.5 nm OSA spectral resolution.

Fig.3.9 shows the normalized spontaneous emission spectral density measured by the OSA1. The short wavelength part of the above spectrum was measured by a liquid Nitrogen cooled InGaAs detector which was used with a Horiba Jobin Yvon spectrometer, while the long wavelength part was measured with the Anritsu OSA. It indicates that the peak emission is at 1537 nm with the 13 dB (5%) bandwidth extending from 1470 nm to 1600 nm. Following the theory outlined in Ref. 8, the band structure of ($^4I_{13/2}$) and ($^4I_{15/2}$) levels of Er^{3+} ions in GaN can be illustrated in the inset (a) of Fig. 3.9. In this diagram, the ground state and the 1st excited state are split into eight and seven equally spaced sub-levels, respectively, due to the Stark effect. The transition between the lowest sub-level of the 1st excited state and the highest sub-level of the ground state produces 1600 nm emission wavelength, while the transition from the top of 1st excited state to the bottom of the ground state represents the 1470 nm emission. In addition, we assume that 1537 nm peak emission wavelength corresponds to the transition between the bottom of the 1st excited state and the bottom of the ground state.

With the above assumptions of energy band structure, the spacing between two adjacent sub-levels within each energy band can be easily calculated by,

$$7\Delta E_1 = hc\left(\frac{1}{1537\times10^{-9}} - \frac{1}{1600\times10^{-9}}\right) \tag{3.2}$$

$$6\Delta E_2 = hc\left(\frac{1}{1470\times10^{-9}} - \frac{1}{1537\times10^{-9}}\right) \tag{3.3}$$

Based on this simplified electronic structure, the excitation energy ε defined in the previous sections can be obtained by combining Eq(2.22) and Eq(2.23).

$$\varepsilon = kT \ln\left[\frac{1-\exp(-\Delta E_1/kT)}{1-\exp(-\Delta E_2/kT)}\right]\left[\frac{1-\exp(-d_2\Delta E_2/kT)}{1-\exp(-d_1\Delta E_1/kT)}\right] - \Delta E_{21} \qquad (3.4)$$

With the measured spontaneous emission spectrum shown in Fig.3.9, the absolute values of the emission cross section can be obtained by using Eq.(2.25) with the knowledge of the radiative carrier lifetime τ_e. Then the absorption cross section can be derived from this emission cross-section, using the McCumber's relation of Eq.(2.21) and the excitation energy ε calculated from Eq.(3.4).

Specifically for the band structure of Er:GaN discussed so far, $\varepsilon = 6515.2cm^{-1}$. Note that the measured carrier lifetime $\tau = (1/\tau_e + 1/\tau_a)^{-1}$ consists of a radiative component τ_e and a non-radiative component τ_a. Our previous measurement indicated two time constants, 1.5ms and 2.8ms for carrier decay in the Er:GaN waveguide. The shorter time constant involved non-radiative recombination and carrier up-conversion. The longer time constant is responsible for the radiative recombination. So we used $\tau_e = 2.8ms$ in the calculation of emission cross section.

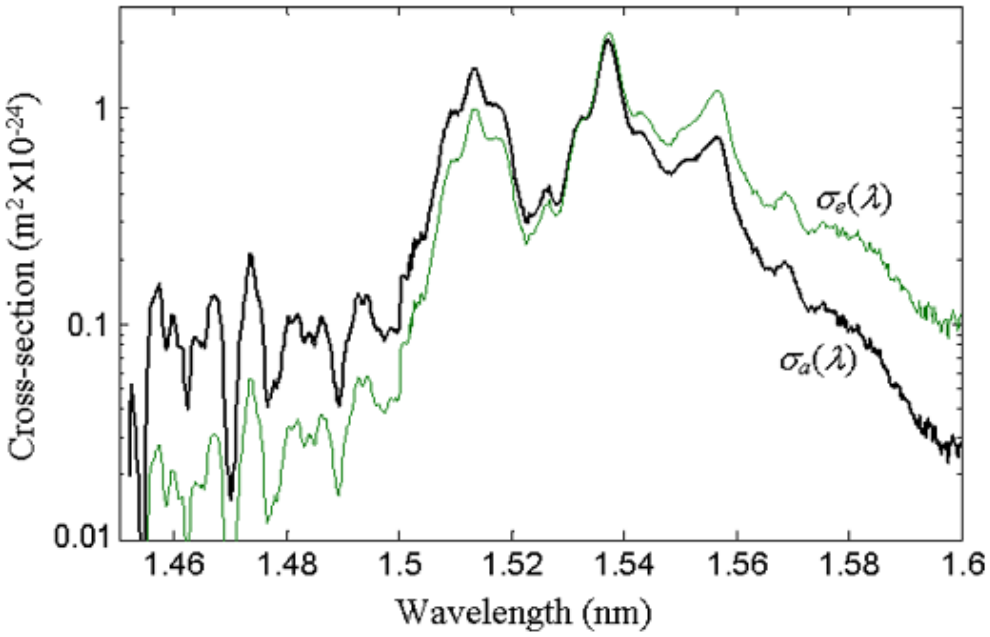

Figure 3-10 Absorption cross section (ACS) and Emission cross section (ECS) for the $^4I_{13/2}$ to $^4I_{15/2}$ transition in an Er:GaN waveguide.

Fig3.10 shows both absorption and emission cross sections determined using the above technique. Although the absolute cross section values of Er:GaN are on the same order of magnitude as those in erbium doped glasses, their cross section spectral shapes are noticeably different. The emission and absorption cross sections shown in Fig3.10 exhibit a number of characteristic peaks due to the regular crystal lattice structure in the GaN material in which the erbium is embedded in, while in erbium doped silica fiber, the cross –section spectra are much smoother because of the amorphous material structure of the glass. Note that in a recent measurement of Er:GaN material at a very low temperature of T=10K, the main emission peak at 1537 nm consists of 4 isolated

emission lines with approximately 1nm (~0.0005eV) wavelength separation between each other, and the results are shown in Figure3.11 [23]

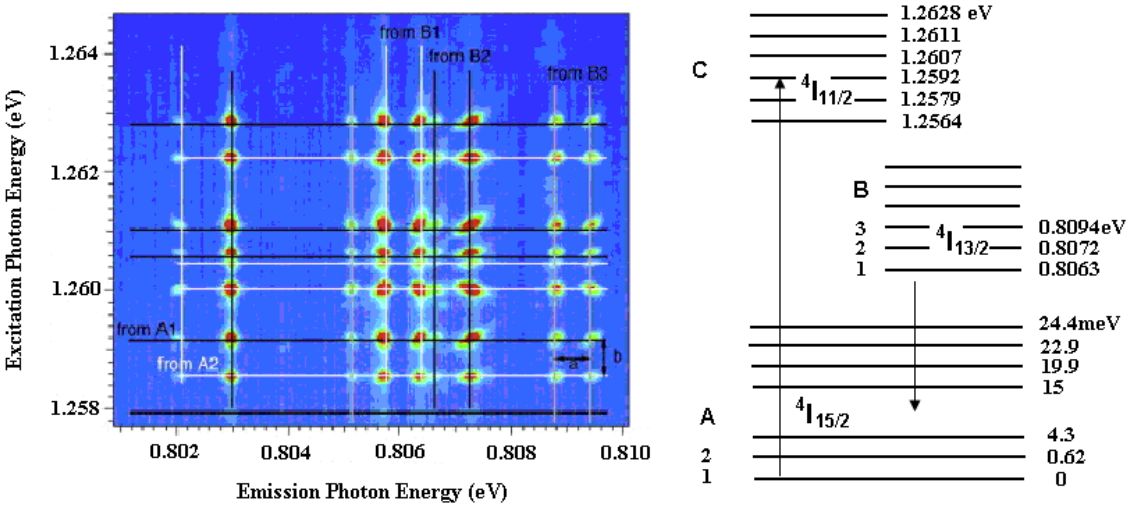

Figure 3-11 Combined emission excitation spectral image plot of Er:GaN [23]. The horizontal lines represent transitions from the ground level to the $^4I_{11/2}$ state, while the vertical lines represent emission peaks from the $^4I_{13/2}$ state to the $^4I_{15/2}$ ground level.

However, in our measurement at room temperature, this spectral splitting was not observed. The inset (b) in Figure3.9 shows the emission peak at 1537 nm measured with 0.5 nm (~0.00025eV) spectral resolution in the OSA, which clearly indicates a continuous emission spectrum. This line broadening is partly attributed to thermally induced lattice vibration of the semiconductor material. In addition, in the waveguide configuration investigated here, non-uniformity of crystal structure along the longitudinal direction of the waveguide may also contribute to this line broadening.

Absorption and emission cross-sections are important parameters which determine the absorption efficiency for the pump and the optical gain for the signal. Since

our measurement extends from 1450nm to 1600nm, the efficiency of 1480 nm pumping can be evaluated, in which a 1480 nm laser was used to pump the erbium ions in the waveguide. In this experiment, the power spectral density of spontaneous emission at 1537nm was measured as the function of the injected pump power, as shown in Figure.3.12. In order to test the accuracy of the cross section values obtained so far, we also calculated the power spectral density of spontaneous emission at 1537 nm versus the pump power 1480nm wavelength based on the following relation,

$$\rho_{ASE} = 2\Gamma\sigma_e(\lambda_s)h\nu_s\int_0^L \frac{N_T P_p e^{-2\alpha z}\sigma_a(\lambda_p)}{P_p e^{-\alpha z}\left[\sigma_a(\lambda_p)+\sigma_e(\lambda_p)\right]+h\nu_p A/\tau}dz \qquad (3.5)$$

where N_T is the doping density of erbium ions. λ_p is the pump wavelength, τ is the carrier lifetime, Γ is the field confinement factor, L is the length of the waveguide, $h\nu_s$ is the signal photon energy, A is the waveguide cross section area, α is the attenuation, and P_p is the pump optical power. According to the cross section values as shown in Figure3.10, the absorption and emission cross-sections at the 1480nm pump wavelength are $\sigma_a(\lambda_p)=1.0\times10^{-21}cm^2$, $\sigma_e(\lambda_p)=3.2\times10^{-22}cm^2$, and emission cross-section at the 1537nm signal wavelength is $\sigma_e(\lambda_s)=2.2\times10^{-20}cm^2$. The calculated results shown as the solid line in Figure3.12 used the following parameters of the waveguide: $N_T=2\times10^{20}cm^3$, $\Gamma=0.198$, $A=9.5\times10^{-8}cm^2$, $\tau=1.5ms$, $L=2.6mm$ and $\alpha=-1.5dB/mm$.

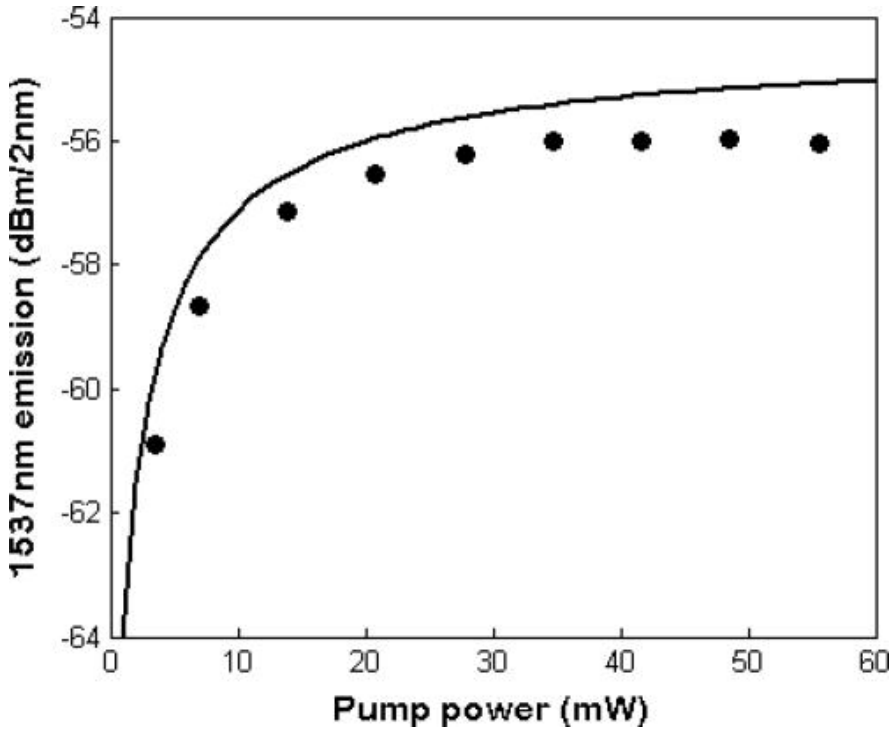

Figure 3-12 Calculated (continuous line) and measured (circles) spontaneous emission power spectral density at 1537 nm wavelength as the function of the injected 1480 nm pump power.

With 50mW pump power, the theoretical power spectral density emitted from the waveguide is -55dBm/2nm which is about 1dB (or 2%) higher than the measured values shown as the open circles in the figure. This reduced emission efficiency is attributed to the non-radiative recombination and Auger recombination for the transition from the metastable level ($^4I_{13/2}$) to the ground level ($^4I_{15/2}$). Overall, the calculated results in Figure3.12 agree reasonably well with the measurement, which validates the cross-section values in Er:GaN waveguides, as well as the pump efficiency at 1480 nm wavelength.

3.4 Measurement of optical gain

In the last two chapters we have described ways to obtain the carrier lifetime and transition cross sections of the Erbium doped GaN waveguide. This chapter discusses the optical gain measurement of the waveguide in the 1550nm window. We used a tunable laser as the signal source, and connected it to one of the inputs of the WDM coupler. The 980nm pump was coupled into the waveguide through the other input of the same WDM coupler. At the other end of the waveguide, a tapered fiber was used to collect the signal optical power emerging from the waveguide. We chose to use a tunable band pass optical filter to select the amplified optical signal while rejecting the wideband spontaneous emission. With the help of a low-noise detector, we transformed the output optical power into an electrical power. In order to evaluate the optical gain of the waveguide introduced by optical pumping, the pump power was switched on and off so that the corresponding change in the output signal optical power can be evaluated with a digital oscilloscope. The setup for this measurement is shown in Fig.3.13.

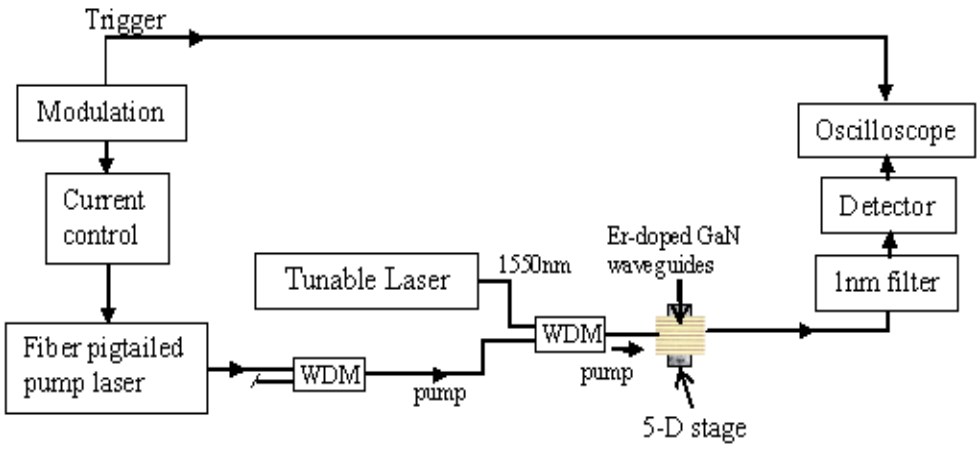

Figure 3-13 Experimental setup for optical gain measurement

During the measurement, we discovered a variation of optical alignment between the tapered fiber and the waveguide every time the pump laser was turned on or off. This variation of alignment turned out to be caused by the movement of the tapered fiber when its plastic coating layer was heated by the strong pump power. This mechanical motion has a time constant in the order of 10ms to 100ms, which causes significant uncertainties of optical coupling condition. In order to minimize this effect, we had to modulate the pump laser at a speed much faster than the thermal effect, so that the instantaneous displacement of the fiber could be neglected.

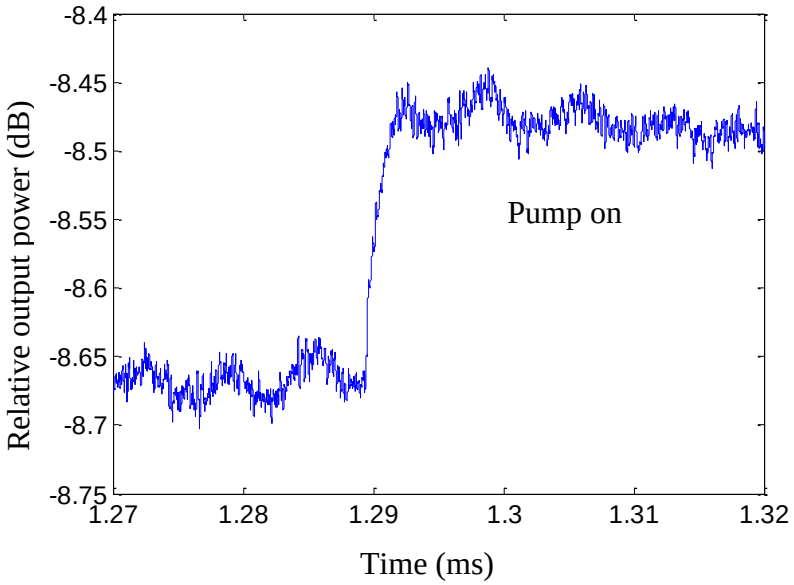

Figure 3-14 Measured Signal Power at 1550nm. The 980nm pump laser was modulated at a high frequency. When the pump power is on, the measured 1550nm signal is larger.

Fig.3-14 shows the relative change of the output optical signal at 1550nm wavelength when the pump was suddenly switched on at the time t = 1.29ms. The figure indicates that the measured signal was about 0.2dB higher when the pump laser was on (about 50mW). So the optical gain at 1550nm was determined to be 0.2dB for this 2.6mm long Er:GaN waveguide. Although the overall gain of 0.2dB is much lower than a typical EDFA, the gain per unit length of this waveguide is 77dB/m, which is at least an order higher than that in an erbium-doped fiber can provide. Further improvement is expected through the reduction of waveguide attenuation and the increase of Erbium doping density.

CONCLUSION

In this thesis, we have reviewed the basic concepts of fiber-optic communication, optical networks and various basic photonic components. Among the basic components, we have particularly focused on the fundamental principles and applications of optical amplifiers and planar optical waveguides. In order to achieve integrated optical circuits with smaller size, we have emphasized our interest in Erbium doped GaN waveguide. The theories and methods to evaluate the Erbium doped fiber amplifiers are reviewed, and we have also studied the techniques and design principles of planar optical waveguide. Then we reviewed a number of popular techniques of determining the transition cross sections in rare earth element doped materials.

As a wide band gap semiconductor (WBGS), GaN has shown a remarkable advantage over other semiconductor materials for its high structural and thermal stability. Meanwhile, the higher refractive index of GaN makes it possible to be used for small size integrated optical circuits, compared to traditional silica optical circuits. The excitation mechanism in Er doped GaN was also discussed. Our main focus in this thesis is the measurement of photoluminescence as well as the determination of some important physical parameters, such as carrier lifetime and transition cross sections. These parameters are essential to determine the characteristics of Erbium doped waveguide amplifiers.

Based on the simulation results using Beam Propagation Method, we designed the structure of the Er doped GaN waveguide. We have calculated the fundamental mode profile that can propagate in the waveguide, and determined the overlap factor of mode

power in Er doped layer. For our experiment, we started with the calibration of all the devices and the build-up of the measurement system. By optimizing the optical alignment we were able to couple sufficient pump power into the Er doped waveguide. We measured the amplified spontaneous emission coming out of the device with an optical spectrum analyzer, and acquired the emission spectra for both 980nm and 1480nm pumping.

In order to determine the carrier lifetime, we used a tunable band-pass filter to select the ASE signal at 1537nm, and measured the dynamic response with a low-noise detector and a digital oscilloscope. Finally, we obtained the carrier life by fitting the decay curve to exponential curves. A shorter carrier lifetime of 1.5 ms and a longer one of 2.8ms were determined, and the non-exponential decay indicated a cooperative up conversion at high pump power. This carrier lifetime is slightly shorter than that in EDFA due to the interaction between the erbium ions and the semiconductor lattice structure. But this carrier lifetime is significantly longer than that in a typical semiconductor optical amplifier which is in the nanosecond regime.

We used a convenient procedure to determine the emission and absorption cross sections in the Er:GaN waveguide sample. The emission cross section was obtained with the Füchtbauer–Ladenburg equation based on the measured spontaneous emission spectrum and the carrier lifetime. The absorption cross-section was then derived from the emission cross-section through their relation provided from the McCumber's theory. The absolute cross-section values measured on Er:GaN are similar to those in erbium-doped glasses, while their cross-section spectral shapes are noticeably different. Because of the

crystal lattice structure in the semiconductor matrix, relatively narrow spectral lines exist in cross-section spectra of Er:GaN waveguides. The efficiency of converting 1480 nm pump into 1537 nm emission was measured, which agrees with the results calculated using the emission and absorption cross-sections, and thus validates the cross-section values. The measurement of carrier lifetime and transition cross sections of Er:GaN is very important when modeling light emitting devices and erbium doped optical amplifiers. However, the project described here shows that the confinement factor of the waveguide can be further improved. In addition, the attenuation introduced by the crystal lattice defects might also be decreased through the improvement of the fabrication process.

References

[1] GOVIND P. AGRAWAL fiber optic communication systems 3rd Ed, (John Wiley & Sons, Inc., New York, 2002)

[2] Rongqing Hui, Maurice O'Sullivan, Fiber Optic Measurement Techniques 1st Ed, (Academic Press, 2008)

[3] Rajiv Ramaswami and Kumar N. Sivarajan, Optical Networks, A Practical Perspective, 2nd Ed, Academic Press, San Francisco, 2002

[4] Gerd Keiser, Optical Fiber Communications 3rd Ed, (McGraw-Hill, Boston, 2000)

[5] E. Desurvire, Erbium-doped Fiber Amplifiers: Principles and Applications, John Wiley & Sons, 1994.

[6] P.C. Becker, N.A. Olsson, and J.R. Simpson, Erbium-Doped Fiber Amplifiers: Fundamentals and Technology (Academic, San Diego, CA, 1999)

[7] R.J. Mears, L. Reekie, I.M. Jauncey, and D.N. Payne, "Low Noise Erbium-Doped Fibre Amplifier Operating at 1.54 μm" Electron.Lett. 23, 1026 (1987)

[8] W. J. Miniscalco,"Erbium-doped glasses for fiber amplifiers at 1500 nm" IEEE J. Lightwave Technol.9, 234 (1991).

[9] M.J Connelly, Semiconductor Optical Amplifiers, Springer, 2002.

[10] C. Ugolini, N. Nepal, J. Y. Lin, H. X. Jiang, and J. M. Zavada, "Excitation dynamics of the 1.54 μm emission in Er doped GaN synthesized by metal organic chemical vapor deposition" Appl. Phys. Lett. 90, 051110 (2007).

[11] Q. Wang, R. Hui, R. Dahal, J. Y. Lin, and H. X. Jiang, "Carrier lifetime in erbium-doped GaN waveguide emitting in 1540 nm wavelength" APL.97, 241105 (2010).

[12] D. E. McCumber, Phys. Rev. 134, A299 (1964).

[13] W. J. Miniscalco and R. S. Quimby, "General procedure for the analysis of Er^{3+} cross sections" Opt. Lett. 16, 258 (1991).

[14] J. A. La´ zaro, J. A. Valles, and M. A. Rebolledo, "Determination of emission and absorption cross sections of Er3+ in the Ti:LiNbO3 waveguides from Transversal fluorescence spectra", Pure Appl. Opt. 7, 1363 (1998).

[15] R. Dahal, J. Y. Lin, H. X. Jiang, and J. M. Zavada, "1.54 μm emitter and optical amplifier based on Er doped InGaN/GaN, " Appl. Phys. Letter 124, 115 (2010).

[16] N. Woodwarda, V. Dierolfa, J.Y. Lin, H.X. Jiang and J.M. Zavada, "Optical and magneto-optical properties of erbium doped InGaN and GaN epilayers," Optical materials, 33,1059 (2011).

[17] C. Y. Chen, S. Wen, and S. Chi, "Measuring emission cross-section profile of erbium-doped fibre with low input power" Electron. Lett. 30, 889 (1994).

[19] R. G. Wilson, R. N. Schwartz, C. R. Abernathy, S. J. Pearton, N. Newman, M. Rubin, T. Fu, and J. M. Zavada, "1.54-μm photoluminescence from Er-implanted GaN and AlN", Appl. Phys. Lett. **65**, 992 (1994).

[20] J. Michel, J. L. Benton, R. F. Ferrante, D. C. Jacobson, D. J. Eaglesham, E. A. Fitzgerald, Y. Xie, J. M. Poate, and L. C. Kimerling, "Impurity enhancement of the 1.54-μm Er^{3+} luminescence in silicon," J. Appl. Phys. **70**, 2672 (1991).

[21] M. Garter, J. Scofield, R. Birkhahn, and A. J. Steckl, "Visible and infrared rare-earth-activated electroluminescence from indium tin oxide Schottky diodes to GaN:Er on Si ," Appl. Phys. Lett. **74**, 182 (1999).

[22] J. M. Zavada, S. X. Jin, N. Nepal, H. X. Jiang, J. Y. Lin, P. Chow, and B. Hertog, "Electroluminescent properties of erbium-doped III–N light-emitting diodes," Appl. Phys. Lett. **84**, 1061 (2004).

[23] N. Woodward,V. Dierolf, J.Y. Lin, H.X. Jiang, J.M. Zavada, Optical and magneto-optical properties of erbium doped InGaN and GaN epilayers

[24] A Zendehnam, M Mirzaei, A Farashiani and. L Horabadi Farahani, "Investigation of bending loss in a single-mode optical fibre", J. Phys., Vol. 74, No. 4, April 2010

[25]Conte, S.D., and deBoor, C. (1972). Elementary Numerical Analysis. McGraw-Hill, New York.

[26] P. N. Favennec, H. L'Haridon, M. Salvi, D. Moutonnet, and Y. LeGuillou, Electron. Lett. **25**, 718 (1989)